Received: 21 December 2015 | Revised: 30 October 2018 | Accepted: 31 October 2018

DOI: 10.1002/nbm.4046

REVIEW ARTICLE

WILEY NMR IN BIOMEDICINE

Fast data acquisition techniques in magnetic resonance spectroscopic imaging

Rohini Vidya Shankar[1] | John C. Chang[2,3] | Houchun H. Hu[4] | Vikram D. Kodibagkar[1]

[1] School of Biological and Health Systems Engineering, Arizona State University, Tempe, AZ, USA

[2] Banner M D Anderson Cancer Center, Gilbert, AZ, USA

[3] School for Engineering of Matter, Transport and Energy, Arizona State University, Tempe, AZ, USA

[4] Department of Radiology and Medical Imaging, Phoenix Children's Hospital, Phoenix, AZ, USA

Correspondence
Vikram D. Kodibagkar, PhD, School of Biological and Health Systems Engineering, Arizona State University, Tempe, AZ 85287, USA.
Email: vikram.kodibagkar@asu.edu

Magnetic resonance spectroscopic imaging (MRSI) is an important technique for assessing the spatial variation of metabolites in vivo. The long scan times in MRSI limit clinical applicability due to patient discomfort, increased costs, motion artifacts, and limited protocol flexibility. Faster acquisition strategies can address these limitations and could potentially facilitate increased adoption of MRSI into routine clinical protocols with minimal addition to the current anatomical and functional acquisition protocols in terms of imaging time. Not surprisingly, a lot of effort has been devoted to the development of faster MRSI techniques that aim to capture the same underlying metabolic information (relative metabolite peak areas and spatial distribution) as obtained by conventional MRSI, in greatly reduced time. The gain in imaging time results, in some cases, in a loss of signal-to-noise ratio and/or in spatial and spectral blurring. This review examines the current techniques and advances in fast MRSI in two and three spatial dimensions and their applications. This review categorizes the acceleration techniques according to their strategy for acquisition of the *k*-space. Techniques such as fast/turbo-spin echo MRSI, echo-planar spectroscopic imaging, and non-Cartesian MRSI effectively cover the full *k*-space in a more efficient manner per T_R. On the other hand, techniques such as parallel imaging and compressed sensing acquire fewer *k*-space points and employ advanced reconstruction algorithms to recreate the spatial-spectral information, which maintains statistical fidelity in test conditions (ie no statistically significant differences on voxel-wise comparisions) with the fully sampled data. The advantages and limitations of each state-of-the-art technique are reviewed in detail, concluding with a note on future directions and challenges in the field of fast spectroscopic imaging.

KEYWORDS

compressed sensing, echo-planar spectroscopic imaging, *k*-space trajectories, magnetic resonance spectroscopic imaging, parallel imaging, sensitivity encoding, wavelet encoding

Abbreviations used: 2D, two dimensional; 3D, three dimensional; 4D, four dimensional; ACS, auto-calibration signal; CS, compressed sensing; CSI, chemical shift imaging; DWT, discrete wavelet transform; EP-COSI, echo-planar correlated spectroscopic imaging; EPI, echo-planar imaging; EP-JRESI, echo-planar *J*-resolved spectroscopic imaging; EPSI, echo-planar spectroscopic imaging; FFT, fast Fourier transform; FOV, field of view; GRAPPA, generalized autocalibrating partially parallel acquisitions; GRASE, gradient and spin echo; MRSI, magnetic resonance spectroscopic imaging; NAA, N-acetyl-aspartate; NUS, non-uniform undersampling; OVS, outer volume suppression; PEPSI, proton echo-planar spectroscopic imaging; PRESS, point-resolved spectroscopy; PSF, point spread function; SENSE, sensitivity encoding; SI-CONCEPT, spectroscopic imaging using concentrically circular echo-planar trajectories; SNR, signal-to-noise ratio; SPICE, spectroscopic imaging by exploiting spatiospectral correlation; SRF, spatial response function; SSFP, steady-state free precession; STEAM, stimulated echo acquisition mode; SW, spectral width; T_E, echo time; T_R, repetition time; U-FLARE, ultrafast low-angle rapid acquisition and relaxation enhancement.

1 | INTRODUCTION

Many disease processes result in metabolic changes in the cells of the affected tissue or organ. In such diseases, identification and quantification of these metabolic molecular markers can aid in diagnosis and consequently improve therapeutic prognosis. In cancers, rapid cell growth requires increased choline production and glucose consumption.[1] Once malignant, cancer cells also lose tissue specific function, such as decreased production of N-acetyl-aspartate (NAA) in brain tumors and citrate in prostate tumors.[1,2] Similarly, liver diseases often result in increased hepatocellular lipid and stromal fibrosis, which indicate the activity and progression of liver inflammation.[3] Various techniques such as positron emission tomography, ultrasound elastography, and MRI have demonstrated ability as well as clinical utility and promise in measuring these metabolic changes.[1] Magnetic resonance spectroscopic imaging (MRSI, also known as chemical shift imaging or CSI), was first introduced by Brown et al[4] and developed further by Maudsley et al[5]. MRSI is a key tool for measuring and monitoring metabolite concentrations in vivo, and is used in conjunction with other anatomical and functional sequences, such as perfusion and diffusion imaging, to probe the tissue microenvironment. While in vivo MRSI has been demonstrated with other nuclei, ^{1}H MRSI is the spectroscopic imaging technique of choice for imaging in the clinic because of greater hydrogen abundance and commercially available equipment, as compared with ^{13}C, ^{31}P, and ^{23}Na MRSI. Nevertheless, these other nuclei are also very useful in investigating specific metabolic processes.[6-25] Although MRSI can monitor clinically relevant biomolecules, its clinical use is limited by the extremely long acquisition time, limited spatial coverage, and low signal-to-noise ratio (SNR).

The long scan time associated with conventional MRSI, due to multiple phase encoding steps in each spatial dimension, limits its incorporation into routine scan protocols. For example, a clinical MRSI acquisition for a 16 × 16 spatial grid can range from approximately 6 to 12 min depending on the repetition time (T_R), with acquisition times proportional to the total number of voxels acquired, which is also equal to the number of phase encoding steps. This is a key difference compared with conventional MRI, where we utilize frequency encoding along one spatial dimension. The total acquisition time in MRI is thus proportional to the phase encoding steps that are acquired in the remaining spatial dimensions. Furthermore, it is necessary to collect anatomical information in every study as well, increasing the total imaging time further. Shorter acquisition times and increased coverage over the volume of interest are critical to the routine use of MRSI in the clinical setting. Fast MRSI can capture the heterogeneity in metabolite distributions and facilitate the monitoring of dynamic changes in the metabolite concentrations in a more clinically acceptable time frame.[26] Thus, there is a need for fast spectroscopic imaging techniques that make efficient use of the available magnetization for faster spatial encoding in order to reduce the acquisition time, while simultaneously retaining acceptable SNR and spatial resolution. The combination of multichannel RF coils, improved gradients, high-field scanners, and improvements in reconstruction algorithms may help realize these goals.[26]

In recent years, several papers have reviewed in detail the fundamental principles of MRSI and have addressed the latest developments in this rapidly growing field.[26-32] This review focuses on the state-of-the-art techniques that have been developed for the acceleration of scan times, particularly in ^{1}H MRSI. Rapid imaging schemes for numerous MRSI applications will be discussed here, without being restricted to any particular anatomical site. Pulse sequences that facilitate fast spatial and frequency encoding will be reviewed, as well as sophisticated reconstruction algorithms used to reconstruct the spectral data acquired using multiple channels, and non-Cartesian *k*-space trajectories, in ^{1}H MRSI. Preclinical and clinical acceleration studies in ^{31}P, ^{23}Na, and hyperpolarized ^{13}C metabolite imaging will also be briefly discussed in the context of this review.

2 | CONVENTIONAL MRSI

Conventional MRSI has a tedious data acquisition process and requires prolonged scan time. Typically, a single excitation is followed by the application of phase encoding gradients, and subsequently a spectroscopic readout is applied without any gradients.[31] In other words, all points in the time and frequency (k_ω) dimension are sampled for a given location (k_x, k_y, k_z) in *k*-space. The spin system is then allowed to relax and the experiment is repeated until all the phase encoding gradient combinations have been played out, sampling all points in *k*-space. MRSI experiments are typically associated with relatively long scan times due to the large number of phase encoding steps needed to cover *k*-space. The total acquisition time in MRSI depends on the number of phase encodes in each direction, the number of signal averages, and the TR of the pulse sequence employed. Volume selection in MRSI is commonly achieved using the point-resolved spectroscopy (PRESS)[33] or stimulated echo acquisition mode (STEAM) techniques.[5,34] Figure 1 illustrates a two-dimensional (2D) MRSI pulse sequence with a PRESS based acquisition. The three slice-selective RF pulses enable the excitation of three intersecting orthogonal planes. Application of gradients along G_x and G_y enables excitation of a slab while a gradient along G_z defines the slice thickness of the PRESS volume. The second half of the second echo generated at time TE_2 is then sampled. Phase encoding gradients are applied along the *x* and *y* directions to spatially encode the echo to yield a three-dimensional (3D) (k_x, k_y, *t*) matrix, which is then subjected to a spatial and temporal Fourier transform to yield the spectra as a function of location. One can increase the spatial resolution by increasing the number of phase encodes (also equal to the number of points in the spatial dimension) along each *k*-space dimension at the expense of time. This is a significant problem, particularly if 2D and 3D MRSI datasets need to be acquired from large volumes of interest at high spatial resolution and SNR. For example, the acquisition of data for a 16 × 16 × 16 3D spectroscopic volume requires the generation of 4096 spectroscopic signals or *k*-space points. This leads to an acquisition time of approximately 1 h 8 min for TR = 1 s and a single signal average. This is a prohibitively long acquisition time for clinical applications in terms of practicality, patient discomfort, cost, and throughput.

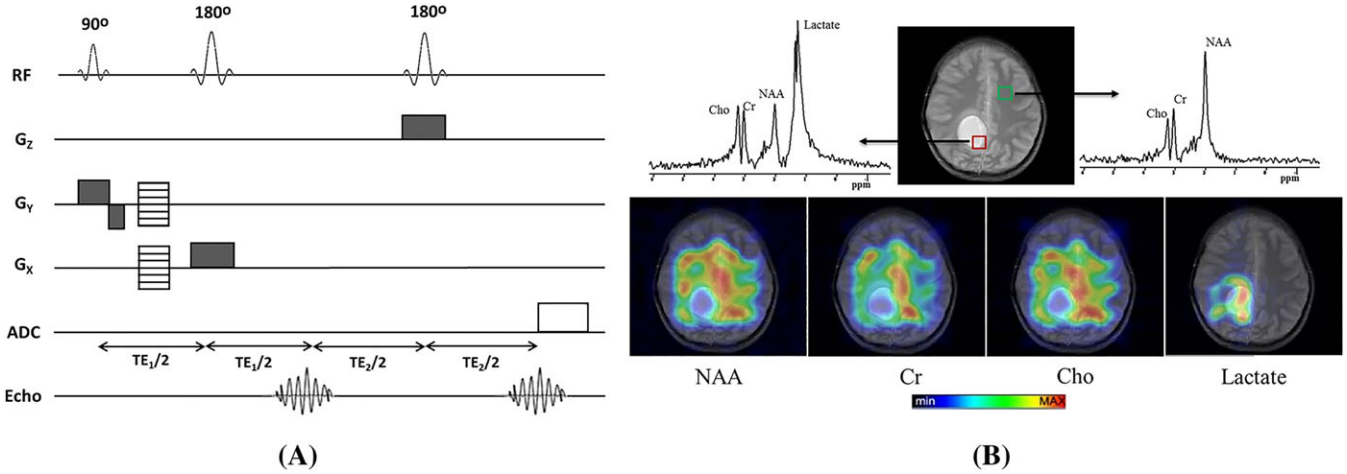

FIGURE 1 Conventional MRSI data acquisition. A, PRESS based volume-selective 2D MRSI pulse sequence with gradient channels G_x, G_y, and G_z, equipped with an analog-to-digital (ADC) converter. The second half of the second echo at time TE_2 is sampled. The total acquisition time in 2D MRSI for a slice in the *z* direction would be $N_xN_yN_{avg}TR$, where N_x and N_y are the numbers of phase encodes (indicated by the horizontally shaded gradient pulses) along the *x* and *y* directions, respectively, N_{avg} is the number of signal averages. B, representative metabolite maps of the major brain metabolites N-acetyl aspartate (NAA), creatine (Cr), choline (Cho), and lactate seen in a brain tumor patient (11 year old male diagnosed with metastatic Ewing's sarcoma), with spectra depicted from normal and tumor voxels. Scan parameters: TE/TR = 46/1500 ms, 16 × 16 × 2048 matrix, one average, total scan time of 9 min. Due to overlapping resonances, the lactate map may include contribution from lipid, especially close to the edge of the brain

Another limitation of MRSI is the inherent low SNR due to low concentrations of the metabolites to be detected. For example, in the normal adult human brain, MR visible metabolites are typically in the range of less than 0.1 to 16.6 mM (as compared with 55 M water).[35] To improve SNR, one can potentially lower the resolution, which will volume-average the signal and potentially lower the signal contrast from the target metabolite with respect to other metabolites. Alternatively, one can increase the number of averages to improve SNR, but at the cost of further increasing the acquisition time. The high concentration of water also necessitates the use of strong water suppression techniques for reliable detection of the smaller metabolites of interest. The stated limitations decrease the enthusiasm of the clinical user to employ conventional MRSI for regular in vivo examinations. Not surprisingly, numerous fast acquisition strategies have been developed for this powerful technique in order to shorten the scan time and increase patient throughput, and these will be discussed in the following section.

3 | FAST MRSI OVERVIEW

As discussed in the previous section, the data at every location in *k*-space are collected with an interval of TR in conventional MRSI, leading to long imaging times. Two main approaches to accelerate data acquisition in MRSI (much like that in imaging) involve either (1) acquiring the full *k*-space (that corresponds to the Fourier transform of the spatial extent of the dataset) in a more efficient manner, timewise, effectively covering more of *k*-space per TR, or (2) acquiring less than the entire *k*-space and estimating the *k*-space data not acquired using reconstruction algorithms. Methods such as turbo MRSI, echo-planar spectroscopic imaging (EPSI), and non-Cartesian MRSI fall into the former category, and achieve acceleration usually by acquisition of more *k*-space per excitation. These techniques, particularly EPSI, have greatly improved the feasibility of including MRSI scans as part of conventional imaging and extended the application of MRSI.

The properties of the Fourier transform and the rectangular extent of *k*-space (corresponding to a rectangular field of view, FOV) enable a sparser sampling scheme by excluding certain portions of *k*-space, although not without affecting the point spread function (PSF).[36] This has led to the later class of fast MRSI techniques, which include circular/elliptical sampling, parallel imaging, compressed sensing (CS), and wavelet encoding. These two classes are not exclusive and can be combined, as in MRI, to gain further speed. We will review techniques in both these categories as well as applications involving combinations of techniques. One could disagree on the inclusion of some of the techniques in one category as opposed to the other. For example, non-Cartesian/spiral MRSI is classified here under more efficient coverage of *k*-space, but it also tends to undersample the *k*-space compared with a conventional rectilinear *k*-space grid. In such cases we have tried to broadly classify according to the dominant effect and do not suggest exclusivity of these two categories to describe any listed technique. Also, it must be pointed out that circular and elliptical sampling schemes are now routinely available on clinical scanners and may be considered as "conventional MRSI". Table 1 summarizes the first implementations of various 2D and 3D fast MRSI techniques that employ novel encoding strategies to reduce the scan time. Also listed are the initially reported limitations, which were subsequently addressed in some cases, as discussed in each section. Since encoding of position in conventional MRSI itself is an extension of that in MRI, most of these acceleration strategies are not MRSI specific. All discussed acceleration approaches were initially applied and tested in MRI before their adoption in MRSI.

TABLE 1 A summary of the first implementations of various fast 2D and 3D MRSI techniques employing different encoding schemes, with acceleration factors as reported in the literature. Early examples of each technique are presented and compared with conventional MRSI. Also listed are the limitations reported by the authors

Reference	Field strength (T)	Anatomy	Acceleration technique	T_R/T_ESW	Scan time	Acceleration factor	Reported limitations
Duyn and Moonen[37]	1.5	Brain	Turbo MRSI 32 × 32 circular *k*-space sampling	2700/200 2000	Conventional MRSI: 27 min Turbo MRSI: 9 min	3×	Loss in spectral SNR and resolution, increased sensitivity to lipid contamination, PSF broadening
Dreher and Leibfritz[38]	4.7	Rat brain	U-FLARE MRSI 64 × 64	1900/170 899	Conventional MRSI: 2 h 9 min 43 s Displaced U-FLARE: 4 min	~32×	SNR loss due to instabilities in the water suppression (factor of $\sqrt{2}$ as compared with phase-cycled U-FLARE)
Dreher and Leibfritz[39]	4.7	Rat brain	GRASE MRSI 64 × 64	1900/19.3 800	Conventional MRSI: 2 h 9 min 43 s GRASE MRSI: 4 min	~32×	Inherent SNR loss by a factor of 2 as compared with conventional MRSI
Posse et al[40]	1.5	Brain	2D EPSI 32 × 32	2000/13 488	Conventional MRSI: 32 min EPSI: 1 min	32×	Limited spectral bandwidth, limited data acquisition window permitting only few slices per T_R, sensitivity to field inhomogeneities, gradient-induced eddy currents
Adalsteinsson et al[41]	1.5	Brain	Spiral MRSI 18 × 18 × 10	2000/144 400	Conventional MRSI: 1 hour 48 min Spiral MRSI: 18 min	6×	Artifacts from lipid contamination, gradient-induced eddy currents, sensitivity to off-resonance-related spatial blurring
Dydak et al[42]	1.5	Brain	SENSE MRSI 32 × 32	1500/136 750	Conventional MRSI: 26 min SENSE SI: 6.5 min	4× ($R_x = R_y = 2$)	SNR loss by a factor of 2 for a SENSE reduction factor of 4 ($g\sqrt{R}$, $g \simeq 1$)
Breuer et al[43]	1.5	Brain	3D GRAPPA MRSI 16 × 16 × 8	1070/135 1600	Conventional MRSI: 36 min 31 s 3D GRAPPA MRSI: 9 min 8 s	4× ($R = 4$)	No limitations reported
Serrai and Senhadji[44]	7	Phantom	2D wavelet-encoded MRSI 8 × 8	2000/70 5000	Conventional MRSI: 4 min 16 s WE-SI: 2 min 2 s	2×	SNR loss by a factor of 2, artifacts observed in empty pixels
Geethanath et al[45]	3	Brain, prostate	CS-MRSI 19 × 22	1000/112 1200	Conventional MRSI: 13 min 56 s CS-MRSI: 2 min 48 s	5×	Retrospective study, reconstruction fails to maintain data fidelity at 10×
Hu et al[46]	3	Prostate cancer (mice)	^{13}C CS-MRSI 16 × 16	215/140 581	Conventional MRSI: 54 s CS-MRSI: 7 s	7.53×	Multinuclear capability, need for hyperpolarizer
Furuyama et al[47]	3	Prostate	NUS 4D EP-JRESI 16 × 16	1500/30 F_1 = 1000, F_2 = 1190	Conventional JRESI: 25 min 36 s (1 average) NUS 4D EP-JRESI: 12 min 48 s (2 averages)	2× (4× undersampling with 2 averages)	Degraded reconstruction accuracy when $R > 5$, spectral smoothing of low-concentration metabolites when SNR is insufficient
Burns et al[48]	3	Breast	NUS 4D EP-COSI 16 × 16	1500/30 F_1 = 1250, F_2 = 1190	Conventional COSI: 20 min NUS 4D EP-COSI: 5 min	4×	Unreliable reconstruction at very low SNR, spectral smoothing of low-concentration metabolites
Wilson et al[49]	3	Calf muscle	NUS 5D EP-COSI 16 × 16 × 8	1500/30 F_1 = 1250, F_2 = 1190	Conventional 5D EP-COSI: 3 h 28 min NUS 5D EP-COSI: 13 min	16×	Residual aliasing artifacts from lipid contamination and unsuppressed water, degradation in spectral resolution

WE-SI, wavelet-encoded spectroscopic imaging.

4 | DOING MORE IN LESS TIME: MRSI TECHNIQUES THAT COVER *k*-SPACE MORE EFFICIENTLY

A straightforward approach to accelerating MRSI involves the acquisition of more *k*-space points within the same T_R, analogous to that performed in accelerated MRI. This could involve acquiring multiple or all lines of *k*-space within a T_R, or the inclusion of novel non-Cartesian trajectories that efficiently traverse *k*-space.

4.1 | Fast spin echo MRSI (turbo MRSI)

Analogous to fast spin echo imaging in conventional MRI, multi-echo imaging (also called turbo MRSI) was one of the first techniques used to accelerate acquisition times, especially in the brain.[27,37] The multi-echo, multi-slice MRSI technique proposed by Duyn and Moonen enabled the acquisition of multiple spin echoes within a single T_R.[37] An echo train length of 4 was used to achieve a fourfold decrease in the acquisition time as compared with the single echo technique. A fast spin echo based spectroscopic imaging sequence is illustrated in Figure 2. However, this technique does have several limitations. The data acquisition readout for spectroscopic imaging needs to be of the order of 0.3–1 s to maintain reasonable spectral resolution, and significant T_2 decay would have already occurred by the time the subsequent echoes were encountered.[27] Consequently, metabolites with short T_2 cannot be observed using this technique. This may force one to accept limited spectral resolution due to fewer echoes and smaller acquisition windows to gain speed. There is also considerable T_2 weighting of different echoes, and metabolites such as lactate need to be imaged carefully, taking into account the fact that the choice of TE modulates the signal appearance of these metabolites.[27] Also, for long echo train lengths, the minimum TR often needs to be increased to accommodate the long readout window required, which tends to offset the time gained in multi-echo encoding. Turbo MRSI has been applied to tissue sampling to evaluate a physiologically based target for heterogeneous lesions in brain biopsies.[50] Yahya and Fallone employed a modified turbo MRSI sequence to facilitate the detection of glutamate and glutamine,[51] while Verma et al implemented a correlated turbo imaging sequence to detect metabolites in the human brain and calf muscle.[52]

Other related multiecho based fast MRSI techniques include the spectroscopic ultrafast low-angle rapid acquisition and relaxation enhancement (U-FLARE)[38,53] and the spectroscopic gradient and spin echo (GRASE)[39] imaging techniques (Figure 3). Spectroscopic U-FLARE acquires "slices" of *k*-space by measuring all data points in the k_x-k_y plane at a given value k_ω after each signal excitation, ie within the TR, using the fast imaging method U-FLARE.[54] There are two different ways to encode the chemical shift. In the first approach, the beginning of the imaging sequence is shifted with respect to the RF excitation in subsequent measurements. Alternately, the time interval between the 90° excitation pulse and the imaging sequence is kept constant and the position of a refocusing 180° pulse, applied within that interval, is incremented to encode the chemical shift. In spectroscopic GRASE, after each signal excitation, all data points from N_{GE} k_x-k_y slices are acquired at different k_ω values by using

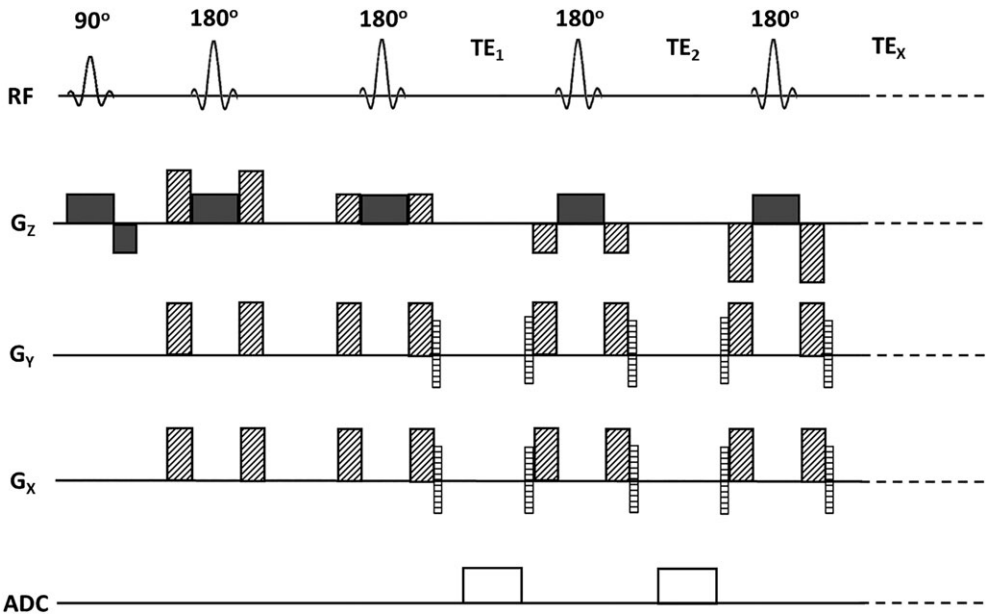

FIGURE 2 A turbo or fast spin echo spectroscopic imaging sequence. This sequence generates and acquires slice-selective spin echoes at echo times TE_1, TE_2, ..., TE_X, in intervals between the 180° RF pulses. Phase encoding gradients (indicated by the horizontally shaded gradient pulses) encode each individual echo in the acquisition interval. Crusher gradients (indicated by the diagonally shaded gradient pulses) around the 180° pulses suppress any unwanted signals. Any unwanted coherences are suppressed with the help of phase encoding rewinders. Gradient pulses depicted by the solid gray boxes represent slice-selective gradients. Additional OVS and water suppression modules can be added before the 90° pulse. Adapted from reference 37

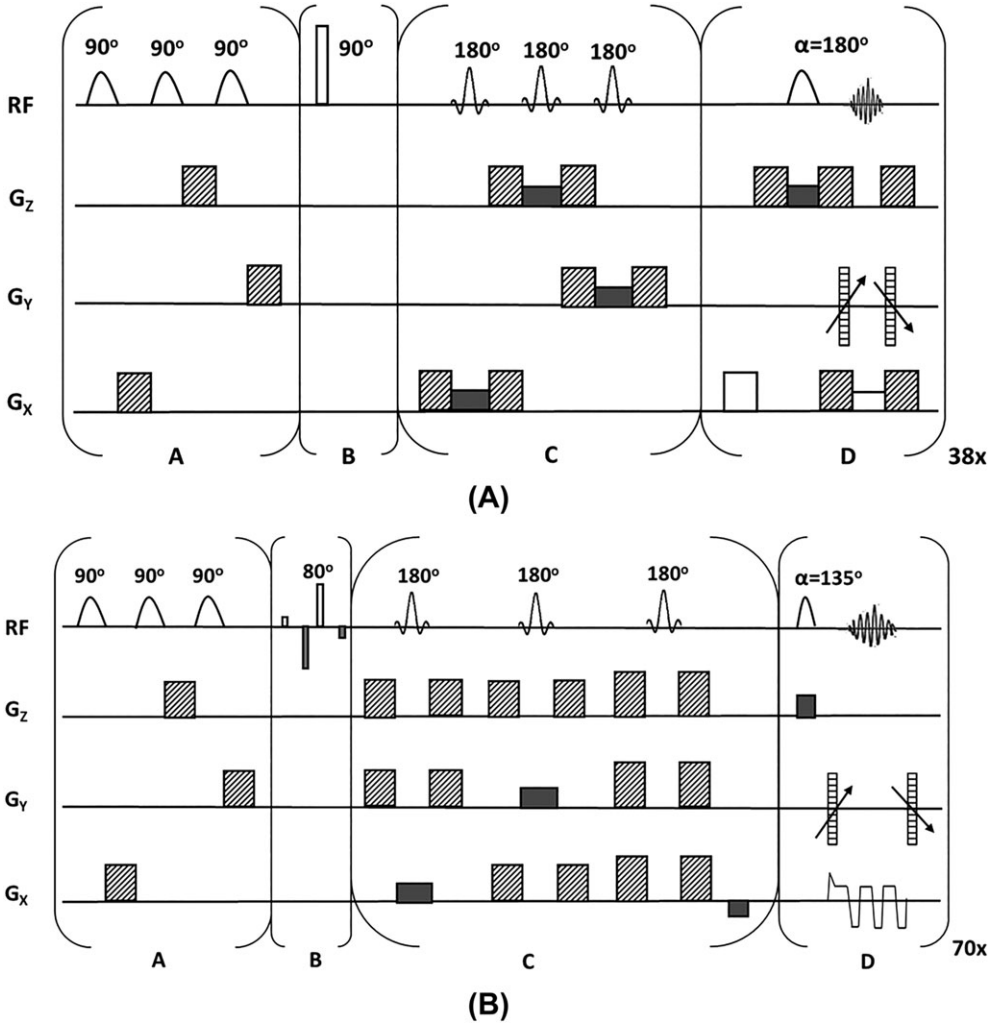

FIGURE 3 Spectroscopic U-FLARE (A) and GRASE (B) imaging pulse sequences with a pre-saturation period A, excitation and evolution period B, an optional localization period C, and readout period D. Phase encoding gradients are denoted using horizontally shaded gradient pulses and spoiler gradients are denoted by diagonally shaded gradient pulses, while solid gray and white boxes depict slice-selective and readout gradients, respectively. Phase encoding gradients are applied before data acquisition and then rewound as indicated by the arrows. Spectroscopic GRASE enables effective homonuclear decoupling, while achieving a lower minimum acquisition time (T_{min}) as compared with the spectroscopic U-FLARE sequence. Adapted from references 39 and 53

a GRASE imaging sequence.[39] The delay between consecutive gradient echoes, which are measured with uniform phase encoding between consecutive refocusing pulses, is the inverse of the spectral width (SW). A refocusing 180° pulse, which is applied within a constant delay between excitation and the GRASE sequence, is shifted for subsequent measurements by an increment N_{GE}/(2 SW) to cover the whole k_ω-k_x-k_y space.

4.2 | EPSI

EPSI or proton echo-planar spectroscopic imaging (PEPSI) in ^{1}H MRSI (Figure 4) was initially proposed by Mansfield[55] and further developed by Posse and co-workers.[40,56,57] The echo-planar imaging (EPI) method[58] was adapted by Mansfield in CSI to facilitate echo-planar shift mapping (EPSM), which was faster than previously employed techniques such as the 3D/4D Fourier transform[5] and the point-by-point topical magnetic resonance method.[59] This resulted in scan times as low as 64 s for 2D acquisition, while maintaining an SNR/unit time and unit volume that was comparable to that obtained using conventional MRSI techniques.[40] The EPSI technique was later extended to 3D for spectroscopic imaging in the human brain at very short T_E (13 ms).[56]

The EPSI technique accelerates the filling of *k*-space (up to three spatial frequencies k_x, k_y, k_z, and time) by acquiring two (any one spatial frequency and time) of the possible four dimensions with each readout.[60] A frequency encoding gradient is rapidly switched during readout to acquire both spectroscopic and spatial data from any one *k*-space dimension, which can subsequently be separated and re-gridded.[60] The acquired echoes can be separated into odd and even echoes, and each even (or odd) echo can be time-reversed and re-gridded to recover the spin echo from the dimension to which the EPI readout was applied. Information from the remaining two spatial dimensions can be then acquired using

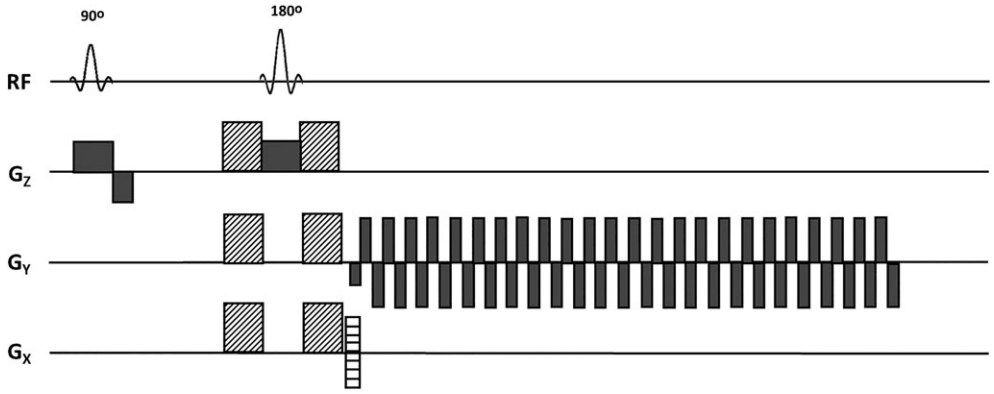

FIGURE 4 A PEPSI pulse sequence with a spin echo excitation section, and an echo-planar spectral readout. Additional OVS and water suppression modules can be added before the 90° pulse. Phase encoding gradients are denoted by horizontally shaded gradient pulses, spoiler gradients are denoted by diagonally shaded gradient pulses, while solid gray boxes depict slice-selective gradients. Adapted from reference 40.

conventional phase encoding. Using EPSI acquisition in 3D, the time required to collect a 16 × 16 × 16 spectroscopic grid is only 16 × 16 s (assuming T_R = 1 s and one average), reducing the scan time from 1 h 16 min to approximately 4 min 16 s. In an early study, 3D EPSI was used along with a fully automated spectral analysis to achieve comparable SNR and superior coverage over a wide region of the brain as conventional MRSI using a 32 × 32 × 16 grid in 15 min/average.[61]

However, EPSI has its share of technical limitations. The use of rapidly oscillating readout gradients places high hardware demands on the gradient system, while the spectral bandwidth is limited by the gradient strength and slew rate.[62] Furthermore, only half the spectral bandwidth is used in conventional EPSI, as the even and odd readout echoes are utilized separately during reconstruction. Limited spectral bandwidth is particularly a problem at higher magnetic field strengths (>3 T), as chemical field dispersion effects increase, leading to spectral aliasing.[62] This can be compensated for by using a cyclic unwrapping method, wherein the aliased portion of the spectrum is cyclically shifted and the region downfield is filled with zeros to obtain a modified spectral distribution.[62] Limited spectral bandwidth in EPSI can also be mitigated using interleaved T_E-shifting at the expense of increased scan time.[63]

There is a drop in the SNR during data acquisition due to the associated short dwell times (resulting in increased bandwidth and hence noise) as compared with conventional MRSI.[60] Corrections of frequency instabilities and local B_0 shift have also been investigated by Ebel et al to limit the line broadening effects seen at higher field strengths in whole-brain 3D EPSI.[64,65] Due to the above mentioned limitations, increased averaging may be required to improve the SNR, which may neutralize the speed gain. Nevertheless, EPSI has proved to be particularly useful in numerous 2D and 3D applications, including those where loss of SNR is acceptable in favor of faster imaging, eg in imaging hyperpolarized probes, where one battles dynamic signal loss due to T_1 relaxation,[66] and 3D ^{1}H spectroscopic imaging of the brain.[67-69]

Numerous preclinical and clinical studies have been conducted using EPSI. On the preclinical front, *J*-coupled and uncoupled spin signals have been detected with high SNR in vivo in the healthy rat brain using a fast 3D EPSI sequence based on the condition of steady-state free precession (SSFP).[70] The new spectral-spatial encoding scheme combined with SSFP enabled rapid mapping of the rat brain in 2 min 23 s in vivo, increasing the appeal of this technique in applications where time-resolved spectroscopic imaging with complete 3D volume coverage is required. EPSI has been used to image prostate cancer in rodent tumor models,[71] wherein it was demonstrated that the vascular environments and heterogenous tissue within solid tumors can be imaged at improved spectral and spatial resolution using EPSI as compared with conventional MRSI. In vivo carbon-edited detection with PEPSI (ICED PEPSI)[72] has been employed for glutamate and glutamine measurement in the rat cortex in vivo at high temporal and spatial resolution, thus improving the imaging of ^{13}C turnover and metabolic fluxes. Multi-band excitation pulses have been employed by Larson et al in dynamic ^{13}C MR spectroscopic imaging to probe hyperpolarized [1-^{13}C] pyruvate dynamics in prostate cancer tumor mouse models, achieving high spatial and temporal resolution.[66]

Du et al also demonstrated that high-resolution EPSI is useful for evaluating blood oxygen level dependent (BOLD) contrast and other susceptibility related effects, as well as for better functional and anatomical imaging of the human brain at 1.5 T.[73] A center out EPSI technique (termed EPSICO) has been developed by Labadie et al to correct for Nyquist ghosts and spurious peaks in the image and spectrum, respectively, to overcome the limitations of the SW in EPSI.[74] Rapid whole-brain mapping using a volumetric multi-shot EPSI technique called MEPSI has been developed by Tyszka and Mamelak for metabolic mapping of the entire brain in under 20 min.[63] Fast T_2 relaxation maps of the cerebral metabolites NAA, creatine, and choline were obtained using PEPSI by Tsai et al at 3 T, to facilitate more accurate quantification of metabolite concentrations in scans employing long T_E.[75]

EPSI has also found applications in ^{31}P MR spectroscopic imaging of the human brain and calf muscle in vivo.[76,77] The detection of phosphorus-containing neurometabolites was demonstrated by Ulrich et al, with the developed 2D ^{31}P EPSI sequence facilitating the rapid acquisition of localized spectra that displayed well-resolved ^{31}P resonances in vivo.[76] The EPSI sequence has also been employed to localize ^{31}P spectra in the human calf muscle.[77] The 2D EPSI measurement proposed by Wilhelm and Bachert enabled a twofold reduction in the measurement time of the PCr signal as compared with conventional CSI acquisition.

Fly-back echo-planar gradient readouts were employed by Cunningham et al to obtain a ninefold reduction in the scan time, with an SNR penalty of 10–30% as compared with conventional phase-encoded MRSI.[78] Fly-back echo-planar readouts have also been used to encode spectroscopic information from the prostate at 3 T, to acquire high-resolution spatial-spectral data in 8.5 min.[79] Srinivasan et al implemented a T_E-averaged PRESS MRSI technique combined with a fly-back echo-planar readout, for the rapid mapping of the 2D spatial distribution of brain glutamate in the clinic.[80] PEPSI has also been adopted to quantitatively map the distribution of total choline in the healthy breast.[81]

4.3 | Non-Cartesian MRSI

k-space is traversed point-wise in a rectilinear manner in conventional MRSI by the choice of phase encoding gradients, leading to long acquisition times. The efficiency of conventional phase-encoded CSI can also be improved by using acquisition or density weighting, as investigated by Greiser and von Kienlin.[82] The *k*-space is sampled in uniform increments in conventional phase encoding, whereas in density-weighted sampling an approximation to a radial weighting function is obtained by varying the distance Δk between neighboring sampling locations. Prior to applying the fast Fourier transform (FFT), interpolation algorithms need to be employed to map the sampling points to a Cartesian grid. Acquisition weighting can significantly improve the profile of the spatial response function (SRF) by suppressing the side lobes, and can achieve higher SNR compared with conventional uniformly weighted CSI. Density weighting was demonstrated by Greiser and von Kienlin in ^{31}P MRSI of the human heart, and can be used to reduce the scan time at a fixed resolution and FOV.

Other, non-Cartesian trajectories such as the spiral and radial, and less common ones such as the rosette, traverse *k*-space more efficiently, enabling faster scans.[41,83,84] These sample the *k*-space non-uniformly as well but have speed as their primary objective (as opposed to improving the SRF). Therefore, non-Cartesian *k*-space sampling has gained increased attention over the years in accelerating MRSI. Spiral MRSI, originally developed by Adalsteinsson et al,[41] traverses the (k_x, k_y) space with high sampling efficiency in a spiral trajectory by applying gradient waveforms along the *x* and *y* axes. The (k_x, k_y, k_f) space is traversed by these gradients with the evolution of time. Rewinding gradient lobes are added immediately after the spiral gradients to facilitate return to the *k*-space origin, as depicted in Figure 5. Multiple spiral shots can be employed to map out the entire *k*-*t* space and collect all data points, resulting in a increase of spectral bandwidth. The collected data are then interpolated onto a Cartesian *k*-space grid by employing a regridding algorithm for conventional Fourier reconstruction techniques.[41] The SNR of the spectra reported by Adalsteinsson et al was found to be comparable to that from conventional MRSI techniques using long T_E and inversion recovery pulses for lipid suppression, demonstrating the value of spiral trajectories for rapid volumetric spectroscopic imaging. A 30% loss in the signal from the metabolites is expected when an inversion time of 170 ms is used to obtain fat suppression of an order of magnitude, due to T_1 relaxation of the inverted metabolite magnetization,[41] and is not specific to the spiral acquisition. As in spiral MRI, variable density spirals can be used to sample *k*-space, thus offering a certain degree of flexibility over the SNR, PSF, and scan time.[85,86] The sampling density is typically highest towards the center of *k*-space, where there is more signal, while sparser sampling is employed towards the peripheral regions of *k*-space. Furthermore, if the origin of each spiral trajectory is at the center of *k*-space during data acquisition, one might be able to compensate for motion artifacts and other instabilities during the experiment, and only produce shot to shot variations in frequency or phase.[87]

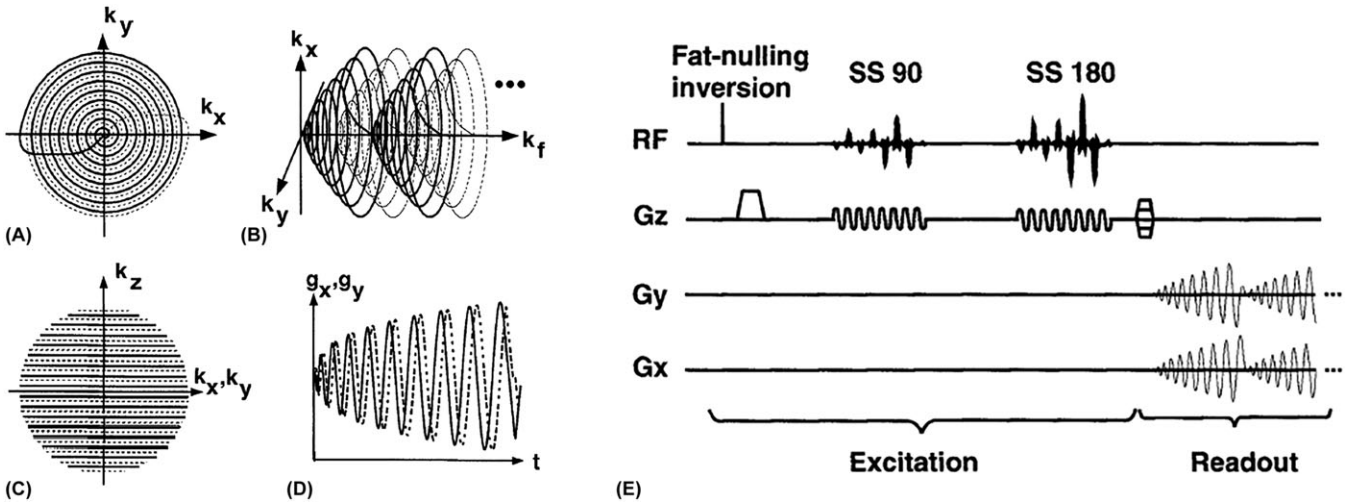

FIGURE 5 The spiral trajectory in *k*-space: Trajectory with a rewinding path back to the origin A, the path traced by the trajectory in (k_x, k_y, k_f) space during the readout time B, phase encoding used to cover the k_z dimension (spherical or ellipsoidal coverage) C, the gradient waveforms g_x (solid) and g_y (dashed) over one period D, and a pulse sequence diagram employing spiral gradients on G_x and G_y to simultaneously encode the *x*, *y*, and *f* dimensions E. fat saturation is achieved via an adiabatic inversion pulse, followed by a spin echo excitation using spectral-spatial 90° (SS 90) and 180° (SS 180) pulses. The *z* dimension is encoded via phase encodes along G_z (denoted by horizontally shaded gradient pulses). The dashed lines in (A) and (C) represent spatial interleaves while those in (B) represent spectral interleaves. Reproduced with permission from reference 41

Some of the constraints and limitations of spiral MRSI are similar to those of PEPSI as discussed in the previous section, since it applies a readout gradient during data acquisition similar to that used in PEPSI. The spiral trajectory tends to be less demanding on the gradient system as compared with the EPI waveform. Artifacts can be minimized by carefully calibrating the gradient system.[27] The need for computationally powerful hardware/software and lack of widespread availability have resulted in limited application of spiral MRSI in the clinic as compared with EPSI. Nevertheless, MRSI sequences employing spiral *k*-space trajectories have found numerous applications over the years. Spiral MRSI has been employed to collect 3D spectroscopic data in the human brain with high SNR and two orders of magnitude reduction in the scan time as compared with conventional CSI.[41,88] On the preclinical front, Hiba et al employed out-and-in spiral trajectories to rapidly collect metabolic information from the rat brain in vivo at 7 T,[89] obtaining spectral quality and spatial resolution comparable to those of standard phase-encoded MRSI. Various innovations have been developed for spiral MRSI and applied to hyperpolarized ^{13}C spectroscopic imaging[90-95] to probe cellular metabolism. These techniques have been used for the sub-second metabolic imaging of ^{13}C pyruvate with the help of undersampled spiral CSI,[92] to volumetrically map the metabolism of ethanol in a rat liver,[93] and for the dynamic mapping of hyperpolarized [2-^{13}C] pyruvate using multiple alternating spectral bands.[95]

Apart from spiral MRSI, there is potential for developing different novel trajectories for the undersampling of *k*-space.[83,84,96-98] Concentrically circular,[83] rosette,[84] and various other arbitrary *k*-space sampling trajectories that can be adopted for MRSI have been investigated[96-98]. Furuyama et al have investigated spectroscopic imaging using concentrically circular echo-planar trajectories, also known as SI-CONCEPT, to speed up the acquisition of MRSI data.[83] Data from all four *k*-space quadrants can be collected within a single acquisition using concentric trajectories, resulting in more efficient data acquisition as compared with rectilinear sampling. The SI-CONCEPT sequence was demonstrated in healthy human volunteers, and compared with the conventional EPSI sequence to obtain quantitatively comparable results with reduced spatial and spectral distortions. The rosette trajectory, investigated by Schirda et al,[84] has modest gradient requirements and is simple to implement, making it an attractive option for accelerating MRSI. Its application was demonstrated in vivo with improvement in the total scan time, and calculations show a higher SNR efficiency as compared with conventional MRSI. When compared with MRSI with sampling on the same *k*-space disk of support, the SNR efficiency is lower.

5 | DOING MORE WITH LESS DATA: FAST MRSI WITH UNDERSAMPLING

An alternative approach to speed up MRSI (or imaging) involves the approximate reconstruction of spectroscopic imaging data from a smaller subset of *k*-space data (acquired in less time than the full *k*-space). As in imaging, the "missing" data is filled using zero-filling and/or iterative nonlinear reconstruction algorithms. While technically the data obtained from these techniques are only an approximation to the "true" data acquired from transforming the full *k*-space, exhaustive validation is usually carried out to show the fidelity of such approaches and their statistical equivalence up to certain acceleration factors depending upon the inherent SNR of the data.

5.1 | Circular and elliptical *k*-space sampling

The circular sampling technique only measures and samples a circular region in *k*-space; the remaining points that have not been collected are zero-filled to produce a Cartesian grid for reconstruction using the FFT.[36] Such a technique not only reduces the scan time, but also improves the overall effect of the PSF. While circular sampling schemes slightly broaden the main lobe of the PSF, a considerable reduction in the number of side lobes can be achieved by density weighting, thus reducing the spatial extent of voxel bleeding.[99] However, this technique has its share of limitations. Circular sampling creates a highly isotropic PSF, leading to increased spatial blurring mainly along diagonals of the image matrix, compared with rectangular sampling, wherein the side lobes of the PSF are propagated along the principal axis.[31,99] Elliptical *k*-space sampling techniques, an extension of circular sampling for cases where the acquisition matrix is non-square, have also been employed to reduce the number of *k*-space points collected.[100] The sampled region of *k*-space is restricted to a central ellipsoidal volume, leading to faster scan times. Elliptical sampling provides better *k*-space coverage compared with circular sampling, particularly in cases where the spatial frequency extent is anisotropic. Spectral definition is accurately maintained, although there is spatial blurring, similar to that in circular sampling. Elliptical sampling combined with density weighting has been investigated by Scheenen et al for accelerating 3D MRSI of the human prostate.[101]

5.2 | Fast MRSI with parallel imaging

Parallel imaging utilizes multiple receiver coils to permit *k*-space undersampling for acceleration of data acquisition.[42,102,103] Reconstruction of raw undersampled *k*-space data into meaningful images in parallel imaging requires accurate knowledge of the coil sensitivities, and can be performed in either the image domain, as in sensitivity encoding (SENSE), or in *k*-space, as in simultaneous acquisition of spatial harmonics (SMASH) and generalized autocalibrating partially parallel acquisitions (GRAPPA).[102] In parallel imaging, a typical tradeoff between data acceleration rate and the robustness of data reconstruction is an inherent loss in SNR dependent on the reduction factor *R*. An additional potential penalty is the geometry, or *g*-factor, which characterizes the ability of the measured coil sensitivity profiles to reconstruct the undersampled *k*-space raw data.[104] Extensive details of the concepts and principles of parallel imaging can be found in the literature.[105,106] All these parallel imaging techniques can be used to speed up MRSI as well.

The application of SENSE to spectroscopic imaging is similar to anatomical imaging. In 2D SENSE MRSI, each *k*-space direction can be undersampled by R_x or R_y, resulting in a final undersampling factor of R_xR_y.[42] This results in an effective $n/R_x \times n/R_y$ matrix from an originally $n \times n$ matrix, resulting in a reduced FOV.[42] Because the effective FOV in SENSE MRSI is smaller than the true FOV, the reconstructed image is aliased (Figure 6).[42] As in anatomical imaging, the unfolding process requires the collection of an accurate sensitivity map from each coil to determine the different weights in the superposed signal.[42,102] Each voxel in the final image is a summation of signals from each coil multiplied by the sensitivity of this coil.[42,102] In the spectral dimension, an aliased image at each sampling frequency needs to be unfolded. Using the notation followed in Reference 103, if *S* denotes the sensitivity matrix, then the unfolding equation described by Pruessmann et al is given by

$$U = \left(S^{H}\psi^{-1}S\right)^{-1}S^{H}\psi^{-1}$$

where *U* is the unfolding matrix, ψ is the receiver noise matrix, and H indicates the transposed complex conjugate. The different weights derived from inaccurate coil sensitivity profiles would result in spurious signal artifacts.[102]

In SENSE spectroscopic imaging, the loss in SNR is directly related to the reduction factor: the SNR drops by a factor of two when $R = 4$. The SNR is also reduced by $1/g$, where *g* is the local geometry factor and is a function of the reduction factor as well as coil configuration. The value of *g*, which is 1 or higher, is an indicator of the ability of the employed coil configuration to separate the aliased pixels and reflects noise amplification due to aliasing.[103] Optimal placement of the coils, which in turn is affected by tradeoffs between single channel noise levels, coil coupling, and geometric and absolute sensitivity relations, can help ensure that *g* is close to 1. SENSE encoding can be extended to the third dimension in 3D MRSI to obtain further decrease in the scan time. SENSE can also be combined with other high-speed MRSI techniques such as multi-echo MRSI to facilitate very fast imaging times. Phased array coils employed for SENSE encoding of the human brain have a better local SNR as compared with conventional volume head coils in the periphery.[27,107] This helps offset the SNR losses that arise from faster scan times. However, phased array coils are extremely sensitive at the scalp (due to proximity), resulting in foldover of the lipid signals into the brain. This requires

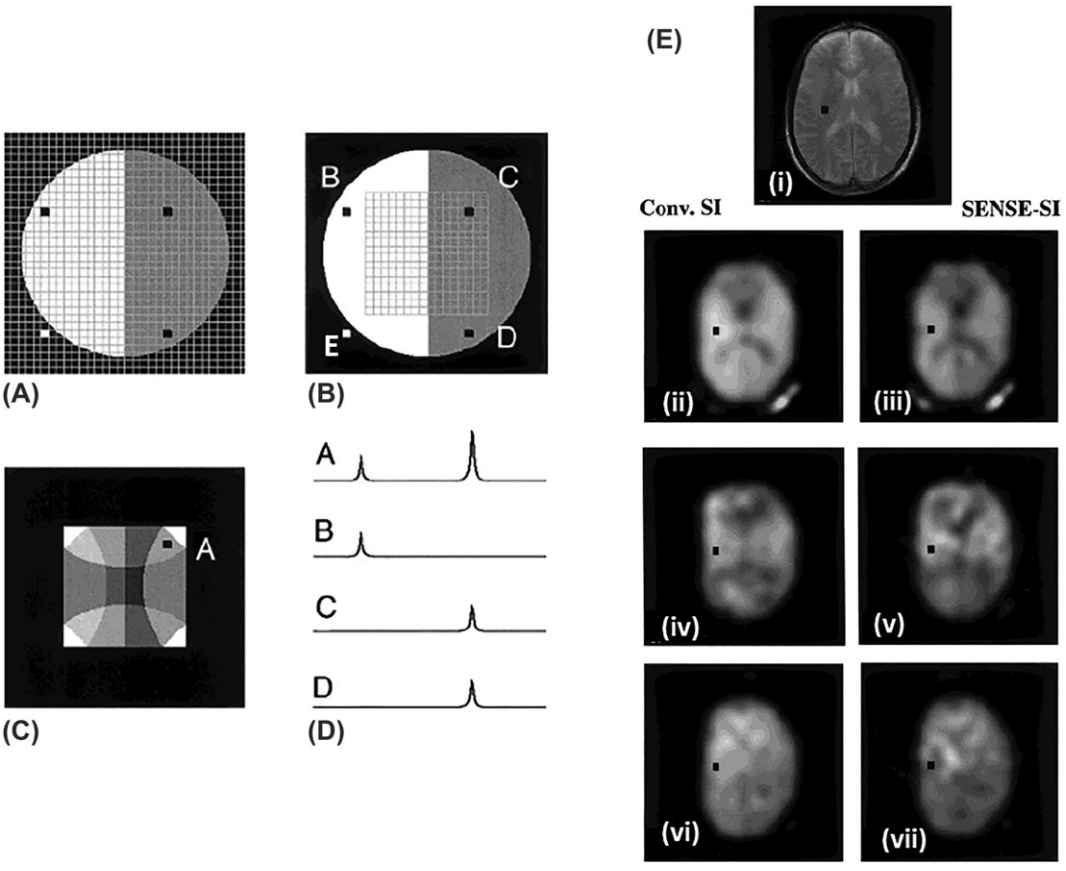

FIGURE 6 The basic principle behind SENSE MRSI. A, As an example, the object depicted contains two different metabolites, as indicated by the color scheme (white and gray regions). B, A SENSE acquisition of a 16 × 16 grid results in a fourfold decrease in the scan time as compared with a conventional 32 × 32 MRSI grid, as only every fourth point in *k*-space is sampled. C, The resulting aliasing artifacts from Fourier reconstruction. D, The SENSE reconstruction unfolds the data from voxel a, which is a weighted sum of the signal contributions from the four voxels highlighted in (B) into its components to obtain the true signal c at that location. E, Representative in vivo scout (i) and metabolite (ii-vii) maps of N-acetyl aspartate (NAA) (ii, iii), creatine (Cr) (iv, v), and choline (Cho) (vi, vii) from conventional (left column, 26 min) and SENSE (right column 6.5 min) MRSI for a 32 × 32 spatial grid. The black voxel was chosen for SNR comparisons between conventional and SENSE spectroscopic imaging. Reproduced with permission from reference 42

powerful lipid suppression techniques to mitigate the demand on the unfolding accuracy of the SENSE reconstruction algorithm.[27,107] Effective lipid suppression can be achieved by using either adiabatic inversion pulses, outer volume crusher coils, carefully selected PRESS/STEAM localization to avoid exciting the peripheral lipid signal, or pre-saturation of the fat signal using outer volume suppression (OVS)[108-117]; the reader is directed to the cited references for a more in-depth discussion on lipid suppression techniques in MRSI. SENSE MRSI has been applied in studies of the human brain[103,118] and in 3D with acceleration along all three dimensions,[119] and for the 3D spectroscopic imaging of gliomas at 3 T.[120]

GRAPPA requires acquisition of the auto-calibration signal (ACS), which is essentially an additional calibration line that is collected along with the reduced data from each coil.[121] The data from multiple lines from all coils can be fit to the ACS line from a single coil, to generate the reconstruction weights that are used to estimate the missing lines. GRAPPA (Figure 7) has been tested in 2D and 3D in both ^{1}H and ^{31}P MRSI by various groups.[43,122] Parallel CSI acquisitions using GRAPPA were tested both in vitro and in vivo to accelerate the MRSI acquisition by a factor of four, while retaining sufficient SNR.[43] GRAPPA eliminates the requirement of collecting separate sensitivity maps, which makes it particularly attractive for studies in ^{31}P MRSI, as demonstrated by Raghavan et al.[122]

5.3 | Wavelet-encoded MRSI

The wavelet encoding technique employs prototype wavelet functions (the discrete wavelet transform, DWT) to identify defined regions in localized space using translations and dilations.[44,123] The slice-selective RF pulse profile is matched to a group of dilated and translated wavelets in MRSI. The spin echo sequence in 2D MRSI wavelet encoding has single and dual band slice-selective excitation and refocusing pulses that have profiles similar to the Haar wavelets.[44] The dilations correspond to increases in the localization gradients, and translations correspond to the frequency shift of the RF pulses. The desired resolution can be achieved by employing a proportional number of dilations and translations. Successive MR signals are acquired from different locations housing regions of variable size, without the T_R waiting time requirement between successive acquisitions, thus reducing the total scan time.[44] The correct spatial distribution of the MR signal is subsequently obtained using an inverse wavelet transform. The general algorithm is shown in Figure 8.

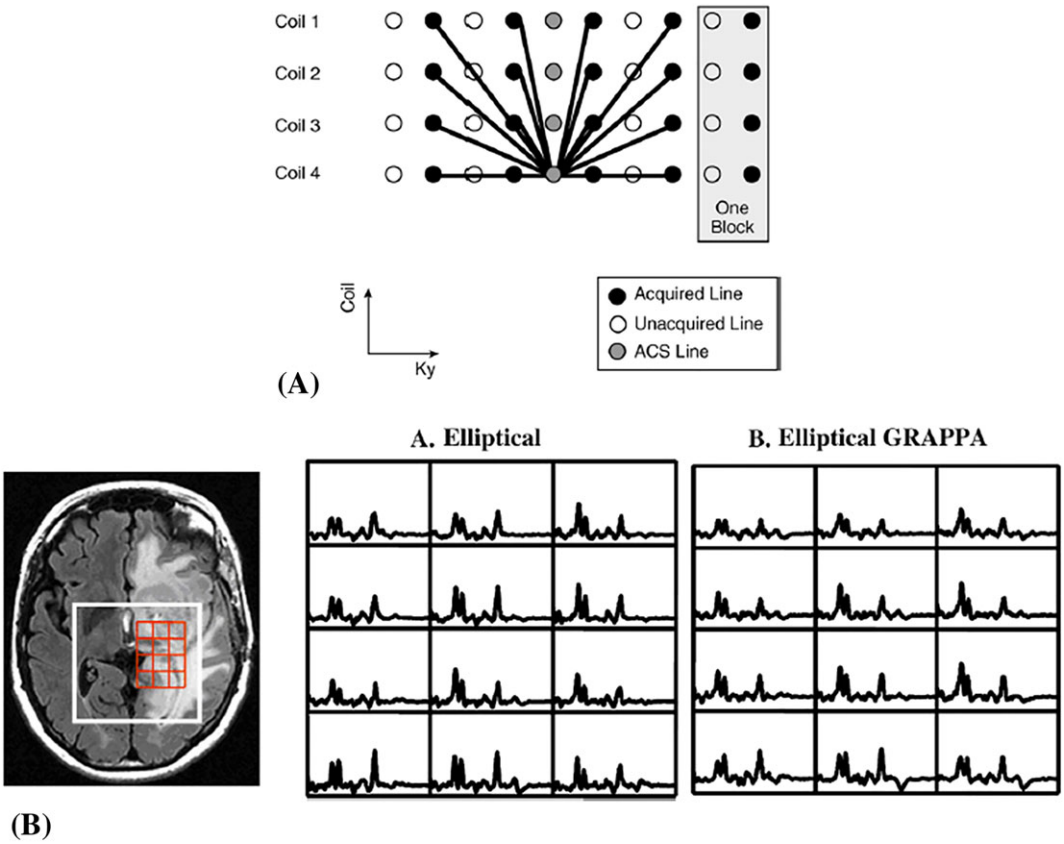

FIGURE 7 A, a schematic diagram of the basic GRAPPA algorithm. In this example, a single ACS line in coil 4 is fitted using four acquired lines. In the GRAPPA technique, a single acquired line along with the missing lines present next to that line constitute a block. A block has been depicted here for an acceleration factor of 2. B, an illustration of the application of GRAPPA to spectroscopic imaging in a glioma patient: Spectra from the tumor region of the chosen PRESS volume of interest for a 12 × 12 × 8 fully sampled elliptical acquisition (i) and a 16 × 16 × 8 elliptical GRAPPA acquisition (ii). Reproduced with permission from references 121 and 100, respectively

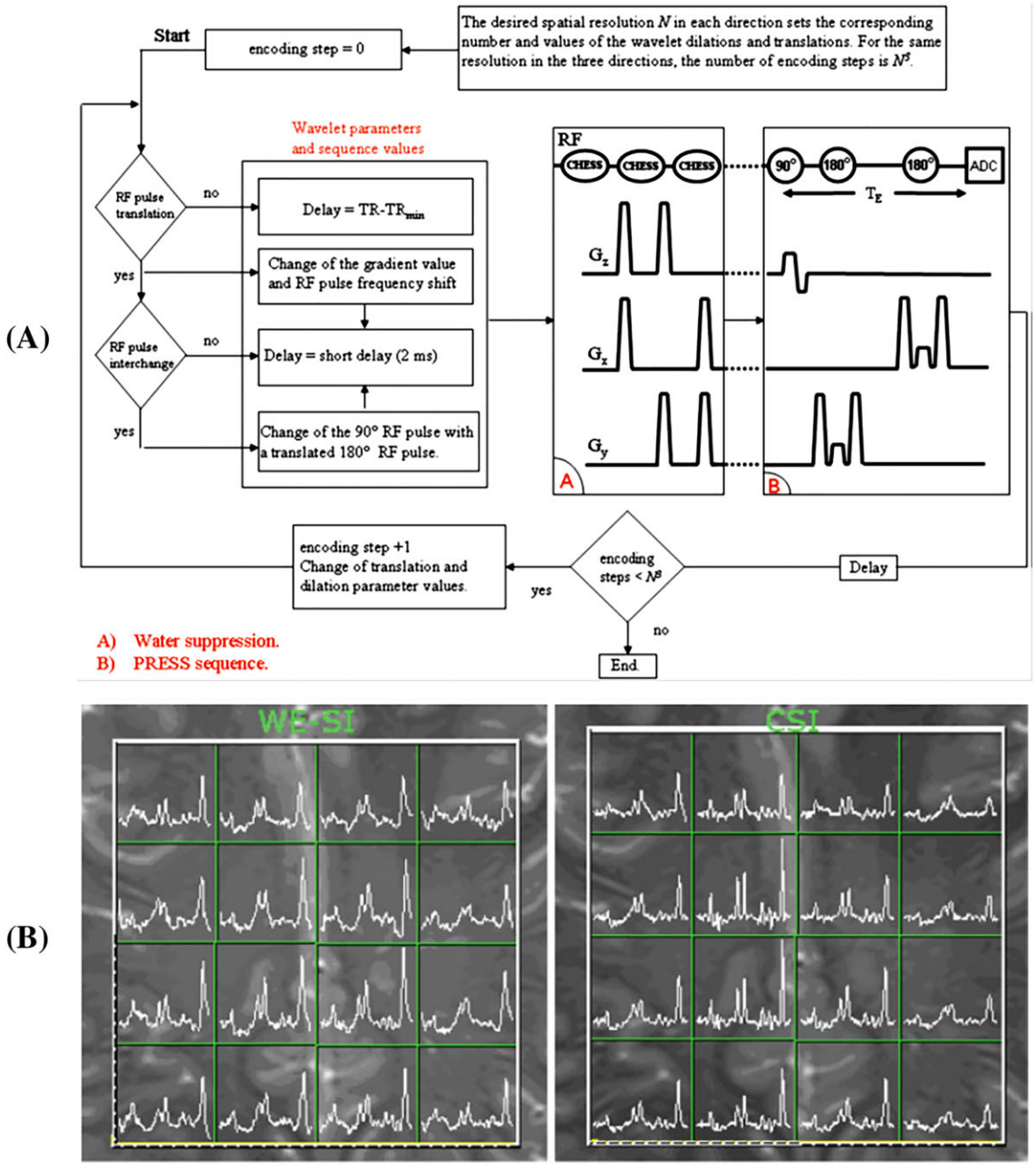

FIGURE 8 A, the wavelet-encoded MRSI algorithm along with the modified PRESS sequence. The sequence parameters such as the delay time, gradient values, and frequency shift of the RF pulses are set by calculating the wavelet dilation and translation parameters at each wavelet encoding step. B, in vivo spectra from healthy volunteers: Wavelet-encoded spectroscopic imaging (left) and corresponding spectra from conventional CSI (right). Scan parameters: T_E/T_R = 75/2000 ms, 4 × 4 × 4 matrix, two averages. Acquisition time for conventional CSI was 4 min 16 s while that for wavelet-encoded CSI was 3 min 20 s. Reproduced with permission from references 123 and 125

Wavelet encoding permits the imaging of only a selected portion of the FOV in a non-contiguous manner. Different subspaces can be excited with no T_R waiting time, accelerating data collection. As the excitation profiles of the RF pulses are modulated to resemble wavelet shapes, there is reduced pixel bleed in the spatial dimensions, which can be observed in the corresponding metabolite maps. The SNR in wavelet encoding is lower than that in Fourier encoding by almost a factor of two, as this technique is limited by the length of the wavelet support.[44] In 2D wavelet MRSI, the SNR drops by a factor of $[(N^2 + 2)/6)^2](4/N^2)$ for an image of size $N \times N$; the authors suggest more averaging to compensate for the signal loss, as the scan time is drastically reduced.[44] Furthermore, in multi-slice imaging, wavelet encoding can be employed to encode the slice dimension, resulting in a higher SNR. Also, a linear combination of prototype wavelet functions, with less spatial localization than Haar wavelets, can be employed to achieve a SNR comparable to that found in conventional Fourier encoding.[124] While wavelet-encoded MRSI preserved the spatial distribution of the signal, paricularly at low resolutions, a few empty pixels had artifacts in the form of residual signals with negative amplitudes.[44] The errors could be attributed to imperfections in the refocusing pulses and the shape of RF profile. Cross-voxel contamination was also observed due to poor shimming. The wavelet encoding technique has been extended to three spatial dimensions in MRSI by Young et al.[123,125] Wavelet-encoded MRSI can also be combined with other parallel imaging approaches to further reduce the acquisition time with minimum loss in the SNR.[126,127]

5.4 | CS-MRSI

CS is a novel approach that exploits the inherent sparsity of medical images in an appropriate transform domain to effectively undersample *k*-space. This in turn reduces the number of samples that are required for reconstruction in MRI and MRSI.[45,128,129] The CS theory successfully predicts that signals can be accurately recovered even when sampling well below the established Nyquist rate, if the signals under consideration are sparse in some transform domain (not just in the time or frequency domains). Data tend to be sparse in multiple dimensions of space and frequency in the wavelet transform domain, thus making this technique particularly suitable for MRSI. Wavelets have been employed to achieve a sparse representation of MRSI data in both the spatial and spectral domains, facilitating the application of CS acquisitions in MRSI.

The CS based reconstruction of undersampled data needs three requirements/steps to be fulfilled. First, the signal under consideration must have a sparse representation in some transform domain (FFT, DWT, etc), ie it should only have a few significant non-zero components in that domain. Second, the signal is then subjected to random (or pseudo-random) undersampling, producing incoherent noise-like aliasing artifacts. Pseudo-random undersampling, which involves sampling the center of *k*-space more densely as compared with the periphery, is preferred to preserve the SNR in MRI/MRSI. Finally, since the problem at hand is ill posed, a non-linear reconstruction algorithm such as the conjugate gradient scheme should be employed to find the optimal solution to a minimization problem, where a functional is constructed, sometimes with multiple components. Typically, the l_1-norm is employed to enforce the sparsity constraint, while the l_2-norm is used to enforce data consistency, in order to minimize the cost function.

CS was first applied to MRI by Lustig et al.[128] The application of CS to ^{1}H MRSI was investigated by Geethanath et al for various acceleration factors, retrospectively.[45] Sampling masks were generated for various acceleration factors, namely 2, 3, 4, 5, and 10, using variable density random undersampling. A 2D probability density function was used to select the random samples, ensuring a denser sampling at the center of *k*-space and sparser sampling of points towards the periphery.[45] The reconstructions at various acceleration factors preserved the fidelity of the metabolite spectrum when compared with the fully sampled conventional MRSI datasets. The algorithm broke down at an acceleration factor of 10, wherein the metabolite peaks began to show increased signal intensities when compared with the conventional MRSI datasets.[45] The reconstruction thus faithfully preserved the prognostic and diagnostic value of the metabolite maps up to an acceleration factor of 5; this retrospective study was an important first step that demonstrated the feasibility of the approach (Figure 9).[45] On the preclinical front, lactate-selective ^{1}H CS-MRSI has been demonstrated in H1975 non-small-cell lung cancer tumors that were subcutaneously implanted, with accelerations up to fivefold maintaining data fidelity with the fully sampled reference dataset (Figure 10).[130]

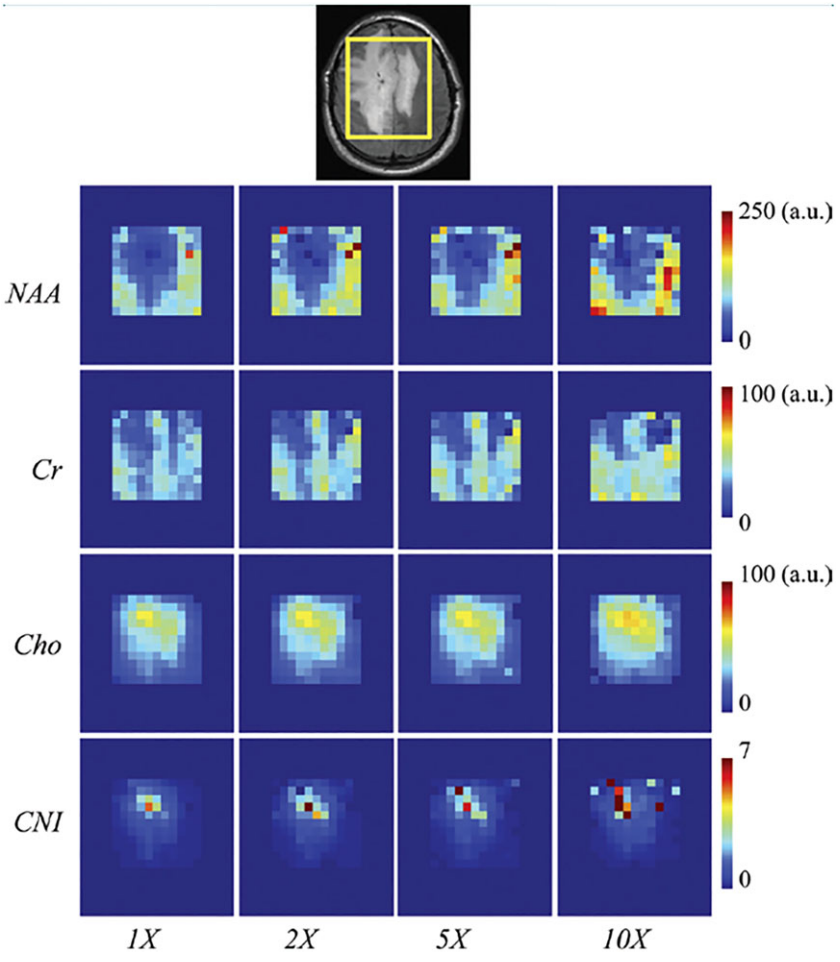

FIGURE 9 Representative metabolite maps of N-acetyl aspartate (NAA), creatine (Cr), and choline (Cho), and choline to NAA index (CNI), demonstrating the retrospective application of CS to ^{1}H MRSI in a brain tumor patient for various acceleration factors. Scan parameters: T_E/T_R = 112/1000 ms, 18 × 21 × 1024 matrix, two averages, total scan time of 12 min 36 s for 1×. Reproduced with permission from reference 45

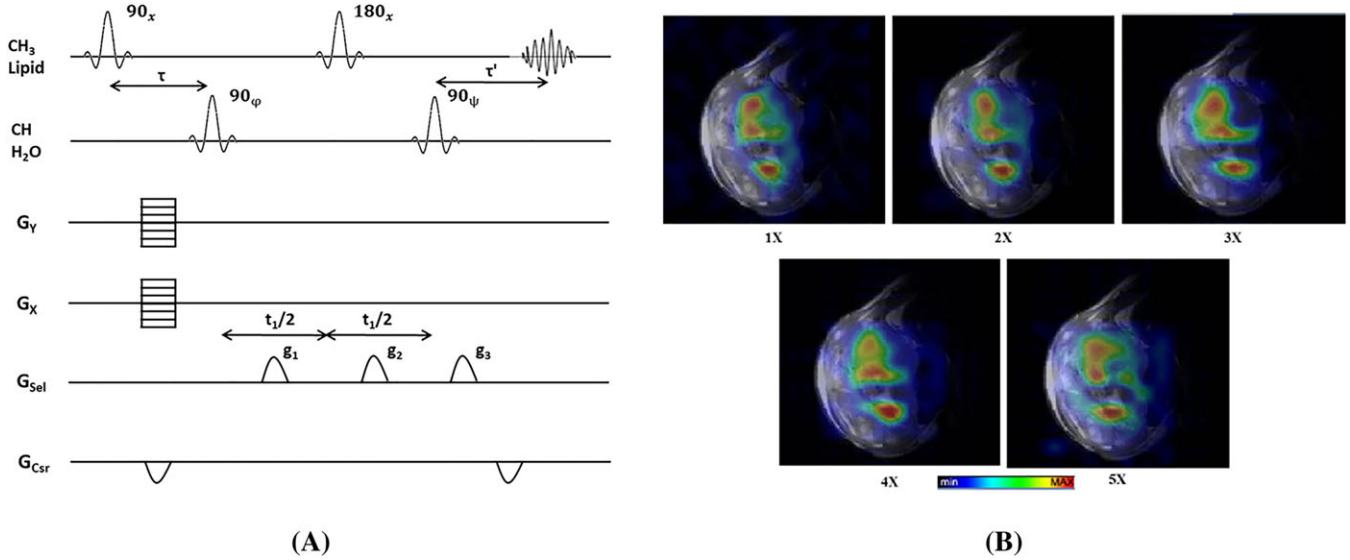

FIGURE 10 A, lactate selective multiple quantum coherence (Sel-MQC) sequence for 2D MRSI with CS based pseudo-random undersampling of the phase encodes G_x and G_y (indicated by horizontally shaded gradient pulses). The first RF channel selectively excites fat and the lactate doublet located at 1.31 ppm. The second RF channel is selective for water (4.65 ppm) and the lactate quartet located at 4.1 ppm. Coherence selection gradients g_1, g_2, and g_3 in the ratio 0:−1:2 allow the multiple quantum coherences of lactate to pass through, while dephasing the single quantum coherences corresponding to water and lipid. B, reconstructed MRSI datasets showing the distribution of lactate in a H1975 tumor (non-small-cell lung cancer) implanted subcutaneously in a mouse thigh for various accelerations. Reproduced with permission from reference 130

A four-dimensional (4D) EPI sequence based on *J*-resolved spectroscopy was used to achieve a high acceleration in vivo, demonstrating the applicability of the multidimensional imaging technique in the clinical setting.[47] Furthermore, CS has been successfully applied to accelerate multi-dimensional spectroscopic imaging studies in the human prostate by Furuyama et al.[47,131-133] 4D echo-planar based *J*-resolved spectroscopic imaging data were collected from a prostate phantom housing physiologically relevant metabolite concentrations. CS undersampling was applied to the indirectly acquired spectral and spatial dimensions and reconstructed using the split Bregman[134] reconstruction algorithm. Retrospective CS reconstructions on in vitro data resulted in a reduction of scan time by up to 80%, while prospectively undersampled data were acquired in healthy prostates achieving a fourfold acceleration factor in vivo (Figure 11).[47]

The CS technique has also been applied to accelerate ^{13}C 3D MRSI, in conjunction with EPSI.[46,135] Typical hyperpolarized spectra only exhibit a few prominent peaks due to negligible background signal from carbon compounds; thus, hyperpolarized ^{13}C spectra are fundamentally sparse in nature.[46,135] Such spectra also have very high SNR due to a more than 50 000-fold increase in the signal due to hyperpolarization. However, there is a limited time-window during which the SNR is very high due to the rapid signal decay, thus necessitating the use of very fast sampling and acquisition techniques. CS, which is best suited for high SNR and sparse data, appears to be an ideal candidate for the conditions mentioned above. The T_1 decay of the hyperpolarized signal restricts the amount of time available for signal acquisition in the time-window when SNR is high, necessitating the use of accelerated imaging techniques for optimal spatial coverage and speed. The sequence proposed by Hu et al achieves an acceleration factor of up to 7.53, and minimal artifacts in the reconstruction for 3D MRSI.[46] The k_ω-k_y-k_x space is pseudo-randomly undersampled

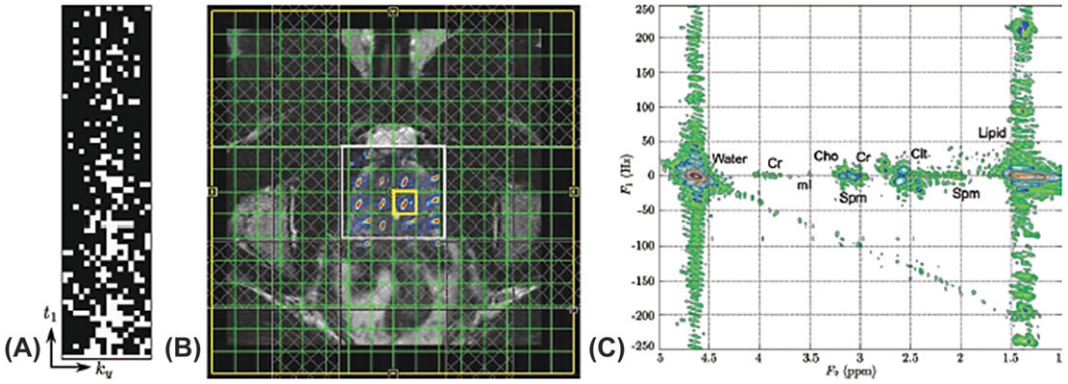

FIGURE 11 An illustration of CS applied to the multidimensional spectroscopic imaging of the human prostate using the EP-JRESI sequence: Mask employing only 25% of the samples necessitated by the Nyquist-Shannon sampling theorem used to undersample the k_y-t_1 plane (the spatial frequency-temporal plane not acquired by the EPSI readout) (a), spatial distribution of the citrate multiplet at 2.6 ppm (B), and *J*-resolved spectrum from the voxel highlighted in yellow showing creatine (Cr), myo-inositol (mI), choline (Cho), spermine (Spm), and citrate (Cit) peaks (C). reproduced with permission from reference 47

by employing *x* and *y* gradient blips during a fly-back readout.[136] The sequence has been tested in simulations, phantoms, and preclinically in vivo in transgenic liver and prostrate cancer murine models.[46] Apart from the decrease in the scan time, a higher temporal and spatial resolution was achieved in the animal models as compared with that possible with conventional EPI techniques.

A time-resolved 3D MRSI technique has been developed by Larson et al[137] to monitor the dynamics of pyruvate conversion to alanine and lactate in a mouse model. This method effectively utilizes the magnetization through the use of multiband excitation pulses in combination with CS for increased acceleration.[137] Random undersampling was applied along four dimensions, namely, frequency (f), time (t), and two spatial dimensions (x, y). Complete volumetric coverage of a mouse was achieved with a temporal resolution of 2 s between each full (x, y, f) scan. The inherent temporal sparsity was also exploited by modifying the CS reconstructions to include a temporal wavelet sparsifying transform. Less hyperpolarization per excitation was achieved by using lower flip angles for the multiband excitation pulses applied to the [1-13C] pyruvate substrate.[137] Thus, this technique enabled dynamic MRSI studies of pyruvate uptake and conversion, contributing to a potentially improved understanding of metabolic changes in cancer imaging. In recent studies, Park et al have used hyperpolarized ^{13}C MRSI to assess heterogeneous metabolic profile variations in orthotopic human glioblastoma xenografts.[138] The variations in the ^{13}C metabolic profiles across different tissue states were captured using high-resolution CS acquisitions, wherein the time gained from a 3.72-fold acceleration was used to achieve a fourfold increase in the spatial resolution as compared with the fully sampled 1× CSI data.[138]

The CS technique has also been applied to ^{31}P MRSI of the human brain.[139] The long scan times associated with ^{31}P MRSI restrict its widespread use in the clinic. Furthermore, ^{31}P MRSI requires larger voxels and increased signal averaging to obtain adequate SNR, as ^{31}P is approximately 15 times less MR sensitive than ^{1}H.[139] The denoising effect of the CS algorithm helps in accelerating MR data acquisition with lower penalty on the SNR. In the study conducted by Askin et al, a higher SNR was observed in the CS reconstructed data, while the peak height ratios of the original and CS datasets were comparable.[139] The long acquisition times associated with conventional ^{31}P MRSI typically do not permit the dynamic imaging of PCr. To overcome this limitation, CS based ^{31}P MRSI has been applied by Parasoglou et al to rapidly capture the kinetics of phosphocreatine (PCr) recovery in the lower leg muscles of humans.[140] The kinetics of the PCr resynthesis rate constant after physical exercise were studied using both retrospective and prospective accelerations with an undersampling factor of 2, achieving a 3D mapping of PCr resynthesis with sufficiently high temporal resolution and speed.

Recent promising preclinical applications of CS MRSI in vivo include ^{19}F 3D spectroscopy in mice,[141] wherein the non-existent background signal in ^{19}F MRSI makes it particularly suited to satisfy the sparsity constraint that is integral to CS. Exogenously administered ^{19}F MRSI has several markers with unique spectral signals that can be readily detected in the presence of a negligible background signal. Kampf et al demonstrated the retrospective application of CS based ^{19}F MRSI both in vitro and in vivo, with the CS reconstructions preserving the fidelity of the data up to an acceleration factor of 8.[141] The first application of high-resolution ^{23}Na spectroscopic imaging in mouse hearts was recently demonstrated by Maguire et al.[142] The ^{23}Na MRSI data from in vivo mouse hearts were prospectively undersampled by 3× and reconstructed using the CS algorithm previously described in Reference 45, to yield undersampled reconstructions that preserved the fidelity of the data.

The non-linear iterative CS reconstruction preserves the spectral line shapes but at the same time causes a gradual smoothing of the spectra with increasing acceleration. This is due to the denoising introduced by the wavelet and total variation terms in the functional of the CS reconstruction algorithm. CS denoising could lead to a smoothing of smaller metabolites that are close to the noise floor in the MRS spectrum, thus presenting the disadvantage of missing these less prominent signals altogether. While most studies tend to focus on the larger metabolites signals such as NAA, Cr, and Cho, there are various other metabolites such as alanine, glycine, glutamate, 2-hydroxyglutarate (2HG), and myo-inositol that are important biomarkers and relatively hard to detect. In such cases, the reconstruction algorithm would need to be tailored to ensure a reliable representation of low-concentration metabolites at higher accelerations, especially when the acquired MRSI data are SNR limited. Other areas of ongoing research involve determining the best pseudo-random undersampling mask tailored to MRSI at each acceleration factor,[143] and investigating the potential impact of CS reconstruction on the low spatial resolution in MRSI.[144]

6 | HYBRID FAST MRSI AND OTHER CONTRIBUTIONS

Various studies have focused on combining acceleration techniques to further reduce scan times and overcome some of the limitations of individual high-speed techniques in MRSI.[105,145-155] Parallel imaging techniques have been combined with CS to reduce the number of acquired data.[145] The method proposed by Dong et al combines CS with the SENSE method to produce a highly accelerated, high-resolution proton MRSI technique.[145] Fu and Serrai have combined the advantages of wavelet encoding with parallel imaging, demonstrating further scan time reduction while preserving the spatial metabolite distribution, in vitro.[148] However, this combination suffers from significant decrease in the intrinsic SNR due to the use of wavelet encoding.[148]

The GRAPPA technique has been combined with ellipsoidal *k*-space trajectories in MRSI to take advantage of the indirect sensitivity estimation based approaches discussed by Banerjee et al.[100] The undersampled data from the elliptical sampling grid were extrapolated to a Cartesian sampling grid using a GRAPPA based operator, and the full *k*-space dataset was subjected to a GRAPPA based reconstruction.[100] These measurements were made on the brains of healthy volunteers at 3 T, and good agreement in the metabolic parameters was obtained between the fully sampled and GRAPPA-sampled datasets.

An ultrafast spectroscopic imaging technique was proposed by Dydak et al, combining SENSE with a multiple spin echo acquisition.[105,146] Posse et al have combined MRSI with parallel imaging techniques to accelerate the acquisition in 3D MRSI of the human brain.[153] PEPSI was combined with 2D SENSE to further shorten the scan times. An eightfold acceleration was achieved in the acquisition of a 32 × 32 × 8 spatial matrix using a 32-channel array coil by employing a 15 ms T_E 3D PEPSI sequence at 3 T.[153] Other high-speed combinations include SENSE-PEPSI,[150,153] spiral MRSI and iterative SENSE,[151] EPSI with SENSE,[152] PEPSI combined with GRAPPA (also termed parallel PEPSI),[154] 3D EPSI using GRAPPA,[155] and miscellaneous other techniques employing parallel imaging and varied *k*-space trajectories.[147,149]

A recently developed hybrid CSI/EPSI technique called SPICE (spectroscopic imaging by exploiting spatiospectral correlation) employs a subspace approach to acquire high-resolution spectroscopic data with good SNR.[156,157] The SPICE technique exploits the property that low-dimensional subspaces tend to contain high-dimensional spectroscopic signals.[156] Sparse sampling of the (*k*, *t*) space is achieved using a hybrid CSI/EPSI sequence that acquires two distinct datasets, D_1 and D_2. In D_1, there is limited *k*-space coverage that is restricted to the central region, while the temporal dimension is fully sampled to determine the temporal basis. In D_2, limited spectral encoding is combined with extended coverage of the *k*-space to identify the high-resolution spatial coefficients. D_1 is acquired using conventional CSI while EPSI is used for the fast acquisition of D_2. The SPICE pulse sequence achieves the simultaneous encoding of two spatial dimensions, along with spectral encoding using echo shifting methods.[156] The reconstruction algorithm extracts the temporal subspace from D_1 and the high-resolution spatial coefficients from the sparse dataset D_2 by using least squares minimization. This technique has been tested in phantoms to obtain a factor of 10 reduction in the scan time with minimal SNR loss as compared with conventional high-resolution MRSI.[156] An optimal selection of the order of separability (model order), regularization parameter, suppression of fat and water resonances, and B_0 inhomogeneity corrections are important for optimizing the SPICE pulse sequence. The reader is directed to the cited references for more in-depth information on the underlying assumptions and limitations of this highly advanced spectroscopic imaging technique.

Hadamard spectroscopic imaging (HSI) is a multivolume technique that employs a finite Hadamard transform of the desired order to achieve spatial localization.[158-160] The HSI method offers the advantage of having a highly controlled PSF that eliminates the voxel crosstalk seen in conventional CSI. Interfering signals from outside the VOI, particularly those from lipid, are inherently suppressed. This results in a better voxel SNR and more optimal SNR/unit time, as in each T_R the entire VOI is excited. HSI also facilitates the acquisition of localized spectra from non-contiguous voxels, and does not require the VOI to be smaller than the FOV, unlike conventional Fourier MRSI, where this would result in aliasing artifacts.[159,161,162] However, this approach is limited by the peak power of the RF pulses, chemical shift displacements, and associated SAR considerations.[162] Various studies have employed either a hybrid 2D CSI-1D HSI (transverse/longitudinal)[159,163,164] or full HSI[162,165-167] scheme for 3D spectroscopic imaging in the human brain.

Apart from the techniques discussed above, parallel imaging has been employed in combination with partial Fourier encoding to accelerate MRSI.[168] The SSFP technique has also been adopted for MRSI and employed in fast ^{31}P MRSI,[169] and the spectroscopic missing pulse-SSFP (spMP-SSFP) based MRSI sequence has been applied for fast ^{1}H MRSI in the brain at 3 T,[170] and at 7 T.[171]. A very recent study introduced a new frequency domain MRSI technique, termed phase-cycled spectroscopic imaging (PCSI),[172] which employed an ultralow-flip-angle balanced steady state free precession (bSSFP) pulse sequence to achieve a 2.5-fold reduction in the scan time.

7 | FUTURE DIRECTIONS

Although MRSI has not found a consistent position in routine clinical protocols, there is little doubt that this technique has proved to be a beneficial clinical tool in numerous cases. Scan time reduction, standardization of data acquisition and processing protocols, and improvements in image quality along with the use of automated software would facilitate the widespread incorporation of this highly useful tool in the clinic. This article has reviewed various innovative and sophisticated high-speed MRSI techniques used to reduce the acquisition time of spectroscopic information. The future holds promise for the development of various hybrid techniques, particularly those involving EPSI, CS, parallel imaging, and novel *k*-space trajectories, to achieve further reduction in scan times and better image quality in terms of the SNR, spatial and temporal resolution, and artifact reduction. The development of scanners equipped with high-performance gradients can help realize the full potential of EPSI. Short T_E, increased sensitivity as compared with conventional CSI, a higher achievable spatial resolution, and simpler reconstruction routines make EPSI a popular technique for fast clinical studies. CS based pulse sequence design also has several potentially beneficial implications in the clinical scenario. Larger matrices and datasets of higher dimensions offer more sparsity to exploit, and the increased room for undersampling could lead to even higher acceleration factors. Furthermore, a key point to note is that the benefits of undersampling along the temporal dimension are not as significant as those along the phase encode dimensions due to the nature of MR signal acquisition. One exception is the EPSI approach, which (even under fully sampled conditions) does not sample the time dimension continuously and hence lends itself to temporal undersampling quite well.[60] However, more sophisticated reconstruction routines could be developed even for conventional readouts to exploit sparsity along the spectral dimension, with a goal of improving SNR or further reducing the scan time.

All the discussed high-speed MRSI techniques have been extensively employed in studies of the brain and to a large extent in the prostate. However, there is limited research on applications to other organs, such as the breast or abdomen. The application of MRSI to many other organ systems is often limited by considerations such as low SNR, increased contamination from peripheral lipid signals (in turn restricting short T_E acquisitions), higher field inhomogeneity, and artifacts due to motion. The main limitation encountered while using fast techniques is the drop in SNR

with increasing acceleration, except in CS, where denoising leads to improved SNR at higher acceleration factors. Other aspects to be considered include eddy current artifacts, the achievable spatial resolution, and the need for fast gradient systems that are often not implementable due to hardware limitations. Non-proton MRSI is also limited by lower MR signal sensitivity, making its clinical translation difficult. Several processing steps are usually required for the complete analysis of MRSI data, and the processing methods vary for different data types as well.[173] This technique is less appealing to the radiologist than other diagnostic imaging protocols (such as perfusion MRI or diffusion MRI) due to a lack of standardization in MRSI acquisition protocols, and the non-availability of common processing and analysis tools for a quick and simple representation of metabolite concentration maps. Automation and quality control are of critical importance in accelerated MRSI techniques, which frequently experience poor spectral quality due to SNR losses, lipid contamination, hardware limitations, and miscellaneous other artifacts. Ultrafast MRSI acquisition techniques also necessitate the use of more sophisticated reconstruction algorithms and complex spatial-spectral analysis to minimize the reconstruction errors from the sparse acquisitions. Implementation of advanced algorithms and routines on the scanner for "on the fly" reconstruction and complex spectral analysis is not a trivial task. One must also take into account the additional time required for reconstruction, post-processing, and display of metabolite maps. The computation time for the more advanced reconstruction routines can range from 6 min 30 s for CS reconstructions[129] to between 10 min/coil and over 4 h in total for the non-uniform undersampling (NUS) 4D/5D echo-planar correlated spectroscopic imaging (EP-COSI) and echo-planar *J*-resolved spectroscopic imaging (EP-JRESI) datasets.[48,49,83,133,174] Furthermore, it is important to note that the time gained from high-speed MRSI techniques may be offset by the need for higher numbers of averages in situations where conventional phase-encoded MRSI is itself SNR limited at the desired spatial resolution. The SNR penalty in conventional MRSI is often large to begin with, and this tends to be further aggravated when employing accelerated MRSI techniques, leading to difficulty in imaging certain anatomical regions (eg the prostate without the use of an endorectal coil).

Another concern in spectroscopic imaging is the effect of the acceleration technique on the PSF and cross-contamination of information between neighboring voxels. In turbo MRSI, the reduced echo duration causes a broadening of the spectral PSF, with phase distortions leading to further PSF degradation.[37] Variable density-weighted trajectories tend to suppress the side lobes of the PSF as compared with uniformly weighted/non-weighted acquisition schemes. Spiral sampling trajectories also tend to have reduced ringing and a narrower central PSF lobe as compared with the phase encoding protocol with elliptical sampling scheme; variable-density spirals can be employed to further reduce the side lobes and ringing.[88] In SENSE spectroscopic imaging, the SRF tends to slightly vary between voxels and is affected by the sensitivity relations.[42] The extent of aliasing in the SRF of a voxel depends on the acceleration or the reduction factor *R* in SENSE, and improper unaliasing of the PSF can lead to residual contamination in the voxels, particularly from lipid-containing regions where the coil sensitivities are poorly defined.[175] In wavelet-encoded MRSI, the PSF is a function of the wavelet shape, and in turn of the RF pulse profile.[123] While the voxel contamination tends to decrease in conventional MRSI with an increase in the spatial resolution, it has been found to remain stable in wavelet-encoded MRSI. In fast MRSI techniques such as CS-MRSI, a coherent broadening of the PSF is avoided due to the incoherent nature of undersampling, resulting in noise-like artifacts.[45,128] Spatial apodization of the MRSI data, which is an important post-processing step, helps in suppressing ringing and the side lobes, at the expense of broadening the PSF and degrading the resolution.

On the other hand, high-speed techniques can help in reducing blurring and streaking artifacts, especially while imaging organ systems that are susceptible to motion. Fast MRSI will also aid in higher volume coverage, and incorporation of specialized spectral editing techniques for mapping metabolites such as lactate and gamma-amino-butyric acid (GABA) that typically require more averaging to obtain the desired SNR. Other techniques such as *J*-resolved spectroscopy and correlation spectroscopy (COSY) could also be incorporated into current clinical protocols to obtain high-resolution spectroscopy data.[48,49,131,174] Thus, either the acceleration offered by high-speed techniques can be employed to decrease the scan time, leading to reduced motion sensitivity and patient discomfort, or the time-saving can be traded for higher SNR/resolution and/or for imaging a larger volume of interest. The reconstruction and quantification of sparsely sampled spectroscopic data on the scanner immediately following data acquisition will also help in improving the practical utility of fast MRSI techniques in current imaging protocols.

ORCID

Rohini Vidya Shankar https://orcid.org/0000-0003-0762-7052
Houchun H. Hu https://orcid.org/0000-0002-0719-1159
Vikram D. Kodibagkar https://orcid.org/0000-0003-1933-8821

REFERENCES

1. Kratz F, Senter P, Chang JC, Gambhir SS, Willmann JK. Imaging techniques in drug development and clinical practice. In: Kratz F, Senter P, Steinhagen H, eds. *Drug Delivery in Oncology: from Basic Research to Cancer Therapy*. Weinheim, Germany: Wiley-VCH; 2011:189-224.
2. Lunacek A, Simon J, Bernt R, Huber M, Plas E, Mrstik C. Increased rate of positive biopsies using a combination of MR-tomography, spectroscopy and diffusion-weighted magnetic resonance imaging prior to prostate biopsies in patients with persistent elevated prostate-specific antigen values: a retrospective analysis. *Urol Ann*. 2013;5(2):76-80.
3. McPherson S, Jonsson JR, Cowin GJ, et al. Magnetic resonance imaging and spectroscopy accurately estimate the severity of steatosis provided the stage of fibrosis is considered. *J Hepatol*. 2009;51(2):389-397.
4. Brown TR, Kincaid BM, Ugurbil K. NMR chemical shift imaging in three dimensions. *Proc Natl Acad Sci U S a*. 1982;79(11):3523-3526.
5. Maudsley AA, Hilal SK, Perman WH, Simon HE. Spatially resolved high-resolution spectroscopy by 4-dimensional NMR. *J Magn Reson*. 1983;51(1):147-152.

6. Chen AP, Kurhanewicz J, Bok R, et al. Feasibility of using hyperpolarized [1-^{13}C] lactate as a substrate for in vivo metabolic ^{13}C MRSI studies. *Magn Reson Imaging*. 2008;26(6):721-726.
7. Larson PE, Hurd RE, Kerr AB, et al. Perfusion and diffusion sensitive ^{13}C stimulated-echo MRSI for metabolic imaging of cancer. *Magn Reson Imaging*. 2013;31(5):635-642.
8. Klomp DW, van de Bank BL, Raaijmakers A, et al. ^{31}P MRSI and ^{1}H MRS at 7 T: initial results in human breast cancer. *NMR Biomed*. 2011;24(10):1337-1342.
9. Zakian KL, Koutcher JA, Malhotra S, et al. Liver regeneration in humans is characterized by significant changes in cellular phosphorus metabolism: assessment using proton-decoupled ^{31}P-magnetic resonance spectroscopic imaging. *Magn Reson Med*. 2005;54(2):264-271.
10. Aguor EN, van de Kolk CW, Arslan F, et al. ^{23}Na chemical shift imaging and Gd enhancement of myocardial edema. *Int J Cardiovasc Imaging*. 2013;29(2):343-354.
11. Bansal N, Germann MJ, Lazar I, Malloy CR, Sherry AD. In vivo Na-23 MR imaging and spectroscopy of rat brain during TmDOTP5- infusion. *J Magn Reson Imaging*. 1992;2(4):385-391.
12. Chmelik M, Kukurova IJ, Gruber S, et al. Fully adiabatic -P 2D-CSI with reduced chemical shift displacement error at 7 T—GOIA-1D-ISIS/2D-CSI. *Magn Reson Med*. 2013;69(5):1233-1244.
13. Chmelik M, Schmid AI, Gruber S, et al. Three-dimensional high-resolution magnetic resonance spectroscopic imaging for absolute quantification of ^{31}P metabolites in human liver. *Magn Reson Med*. 2008;60(4):796-802.
14. Hattingen E, Lanfermann H, Menon S, et al. Combined ^{1}H and ^{31}P MR spectroscopic imaging: impaired energy metabolism in severe carotid stenosis and changes upon treatment. *Magn Reson Mater Phys Biol Med*. 2009;22(1):43-52.
15. Heyne JP, Rzanny R, Hansch A, Leder U, Reichenbach JR, Kaiser WA. ^{31}P-MR spectroscopic imaging in hypertensive heart disease. *Eur Radiol*. 2006;16(8):1796-1802.
16. Kobus T, Bitz AK, van Uden MJ, et al. In vivo ^{31}P MR spectroscopic imaging of the human prostate at 7 T: safety and feasibility. *Magn Reson Med*. 2012;68(6):1683-1695.
17. Kurhanewicz J, Bok R, Nelson SJ, Vigneron DB. Current and potential applications of clinical ^{13}C MR spectroscopy. *J Nucl Med*. 2008;49(3):341-344.
18. Lagemaat MW, Maas MC, Vos EK, et al. ^{31}P MR spectroscopic imaging of the human prostate at 7 T: T_1 relaxation times, nuclear Overhauser effect, and spectral characterization. *Magn Reson Med*. 2015;73(3):909-920.
19. Mirkes C, Shajan G, Chadzynski G, Buckenmaier K, Bender B, Scheffler K. ^{31}P CSI of the human brain in healthy subjects and tumor patients at 9.4 T with a three-layered multi-nuclear coil: initial results. *Magn Reson Mater Phys Biol Med*. 2016;29(3):579-589.
20. Saito K, Matsumoto S, Takakusagi Y, et al. ^{13}C-MR spectroscopic imaging with hyperpolarized [1-^{13}C] pyruvate detects early response to radiotherapy in SCC tumors and HT-29 tumors. *Clin Cancer Res*. 2015;21(22):5073-5081.
21. Schmidt R, Laustsen C, Dumez JN, et al. *In vivo* single-shot ^{13}C spectroscopic imaging of hyperpolarized metabolites by spatiotemporal encoding. *J Magn Reson*. 2014;240:8-15.
22. van der Velden TA, Italiaander M, van der Kemp WJ, et al. Radiofrequency configuration to facilitate bilateral breast ^{31}P MR spectroscopic imaging and high-resolution MRI at 7 tesla. *Magn Reson Med*. 2015;74(6):1803-1810.
23. Varma G, Wang X, Vinogradov E, et al. Selective spectroscopic imaging of hyperpolarized pyruvate and its metabolites using a single-echo variable phase advance method in balanced SSFP. *Magn Reson Med*. 2016;76(4):1102-1115.
24. Weingartner S, Wetterling F, Konstandin S, Fatar M, Neumaier-Probst E, Schad LR. Scan time reduction in ^{23}Na-magnetic resonance imaging using the chemical shift imaging sequence: evaluation of an iterative reconstruction method. *Z Med Phys*. 2015;25(3):275-286.
25. Yen YF, Kohler SJ, Chen AP, et al. Imaging considerations for in vivo ^{13}C metabolic mapping using hyperpolarized ^{13}C-pyruvate. *Magn Reson Med*. 2009;62(1):1-10.
26. Nelson SJ, Ozhinsky E, Li Y, Park I, Crane J. Strategies for rapid in vivo ^{1}H and hyperpolarized ^{13}C MR spectroscopic imaging. *J Magn Reson*. 2013;229:187-197.
27. Barker PB, Lin DDM. In vivo proton MR spectroscopy of the human brain. *Prog Nucl Magn Reson Spectrosc*. 2006;49(2):99-128.
28. Nelson SJ, Vigneron DB, Star-Lack J, Kurhanewicz J. High spatial resolution and speed in MRSI. *NMR Biomed*. 1997;10(8):411-422.
29. Pohmann R, von Kienlin M, Haase A. Theoretical evaluation and comparison of fast chemical shift imaging methods. *J Magn Reson*. 1997;129(2):145-160.
30. Posse S, Otazo R, Dager SR, Alger J. MR spectroscopic imaging: principles and recent advances. *J Magn Reson Imaging*. 2013;37(6):1301-1325.
31. Skoch A, Jiru F, Bunke J. Spectroscopic imaging: basic principles. *Eur J Radiol*. 2008;67(2):230-239.
32. Zierhut ML, Ozturk-Isik E, Chen AP, Park I, Vigneron DB, Nelson SJ. ^{1}H spectroscopic imaging of human brain at 3 tesla: comparison of fast three-dimensional magnetic resonance spectroscopic imaging techniques. *J Magn Reson Imaging*. 2009;30(3):473-480.
33. Bottomley PA. Spatial localization in NMR spectroscopy in vivo. *Ann N Y Acad Sci*. 1987;508:333-348.
34. Salibi N, Brown MA. *Clinical MR Spectroscopy: First Principles*. New York: Wiley; 1998.
35. Govindaraju V, Young K, Maudsley AA. Proton NMR chemical shifts and coupling constants for brain metabolites. *NMR Biomed*. 2000;13(3):129-153.
36. Maudsley AA, Matson GB, Hugg JW, Weiner MW. Reduced phase encoding in spectroscopic imaging. *Magn Reson Med*. 1994;31(6):645-651.
37. Duyn JH, Moonen CT. Fast proton spectroscopic imaging of human brain using multiple spin-echoes. *Magn Reson Med*. 1993;30(4):409-414.
38. Dreher W, Leibfritz D. Improved proton spectroscopic U-FLARE imaging for the detection of coupled resonances in the rat brain in vivo. *Magn Reson Imaging*. 1999;17(4):611-621.
39. Dreher W, Leibfritz D. A new method for fast proton spectroscopic imaging: spectroscopic GRASE. *Magn Reson Med*. 2000;44(5):668-672.
40. Posse S, Tedeschi G, Risinger R, Ogg R, Le Bihan D. High speed ^{1}H spectroscopic imaging in human brain by echo planar spatial-spectral encoding. *Magn Reson Med*. 1995;33(1):34-40.

41. Adalsteinsson E, Irarrazabal P, Topp S, Meyer C, Macovski A, Spielman DM. Volumetric spectroscopic imaging with spiral-based *k*-space trajectories. *Magn Reson Med*. 1998;39(6):889-898.
42. Dydak U, Weiger M, Pruessmann KP, Meier D, Boesiger P. Sensitivity-encoded spectroscopic imaging. *Magn Reson Med*. 2001;46(4):713-722.
43. Breuer F, Ebel D, Ruff J, et al. Parallel 2D and 3D spectroscopic imaging using GRAPPA. *Proc Int Soc Magn Reson Med*. 2006;14:3653.
44. Serrai H, Senhadji L. Acquisition time reduction in magnetic resonance spectroscopic imaging using discrete wavelet encoding. *J Magn Reson*. 2005;177(1):22-30.
45. Geethanath S, Baek HM, Ganji SK, et al. Compressive sensing could accelerate ^{1}H MR metabolic imaging in the clinic. *Radiology*. 2012;262(3):985-994.
46. Hu S, Lustig M, Balakrishnan A, et al. 3D compressed sensing for highly accelerated hyperpolarized ^{13}C MRSI with in vivo applications to transgenic mouse models of cancer. *Magn Reson Med*. 2010;63(2):312-321.
47. Furuyama JK, Wilson NE, Burns BL, Nagarajan R, Margolis DJ, Thomas MA. Application of compressed sensing to multidimensional spectroscopic imaging in human prostate. *Magn Reson Med*. 2012;67(6):1499-1505.
48. Burns B, Wilson NE, Furuyama JK, Thomas MA. Non-uniformly under-sampled multi-dimensional spectroscopic imaging in vivo: maximum entropy versus compressed sensing reconstruction. *NMR Biomed*. 2014;27(2):191-201.
49. Wilson NE, Burns BL, Iqbal Z, Thomas MA. Correlated spectroscopic imaging of calf muscle in three spatial dimensions using group sparse reconstruction of undersampled single and multichannel data. *Magn Reson Med*. 2015;74(5):1199-1208.
50. Martin AJ, Liu H, Hall WA, Truwit CL. Preliminary assessment of turbo spectroscopic imaging for targeting in brain biopsy. *Am J Neuroradiol*. 2001;22(5):959-968.
51. Yahya A, Fallone BG. Detection of glutamate and glutamine (Glx) by turbo spectroscopic imaging. *J Magn Reson*. 2009;196(2):170-177.
52. Verma G, Lipnick S, Ramadan S, Nagarajan R, Thomas MA. Implementation of multi-echo-based correlated spectroscopic imaging and pilot findings in human brain and calf muscle. *J Magn Reson Imaging*. 2011;34(2):262-269.
53. Norris DG, Dreher W. Fast proton spectroscopic imaging using the sliced *k*-space method. *Magn Reson Med*. 1993;30(5):641-645.
54. Norris DG. Ultrafast low-angle RARE: U-FLARE. *Magn Reson Med*. 1991;17(2):539-542.
55. Mansfield P. Spatial mapping of the chemical shift in NMR. *Magn Reson Med*. 1984;1(3):370-386.
56. Posse S, DeCarli C, Le Bihan D. Three-dimensional echo-planar MR spectroscopic imaging at short echo times in the human brain. *Radiology*. 1994;192(3):733-738.
57. Posse S, Otazo R, Caprihan A, et al. Proton echo-planar spectroscopic imaging of J-coupled resonances in human brain at 3 and 4 tesla. *Magn Reson Med*. 2007;58(2):236-244.
58. Mansfield P. Multi-planar image-formation using NMR spin echoes. *J Phys C Solid State*. 1977;10(3):L55-L58.
59. Gordon RE, Hanley PE, Shaw D, et al. Localization of metabolites in animals using ^{31}P topical magnetic resonance. *Nature*. 1980;287(5784):736-738.
60. Mulkern RV, Panych LP. Echo planar spectroscopic imaging. *Concepts Magn Reson*. 2001;13(4):213-237.
61. Ebel A, Soher BJ, Maudsley AA. Assessment of 3D proton MR echo-planar spectroscopic imaging using automated spectral analysis. *Magn Reson Med*. 2001;46(6):1072-1078.
62. Ebel A, Maudsley AA, Weiner MW, Schuff N. Achieving sufficient spectral bandwidth for volumetric 1H echo-planar spectroscopic imaging at 4 tesla. *Magn Reson Med*. 2005;54(3):697-701.
63. Tyszka JM, Mamelak AN. Volumetric multishot echo-planar spectroscopic imaging. *Magn Reson Med*. 2001;46(2):219-227.
64. Ebel A, Maudsley AA, Schuff N. Correction of local B_0 shifts in 3D EPSI of the human brain at 4 T. *Magn Reson Imaging*. 2007;25(3):377-380.
65. Ebel A, Maudsley AA. Detection and correction of frequency instabilities for volumetric ^{1}H echo-planar spectroscopic imaging. *Magn Reson Med*. 2005;53(2):465-469.
66. Larson PE, Bok R, Kerr AB, et al. Investigation of tumor hyperpolarized [1-13C]-pyruvate dynamics using time-resolved multiband RF excitation echo-planar MRSI. *Magn Reson Med*. 2010;63(3):582-591.
67. Ebel A, Maudsley AA. Improved spectral quality for 3D MR spectroscopic imaging using a high spatial resolution acquisition strategy. *Magn Reson Imaging*. 2003;21(2):113-120.
68. Ebel A, Schuff N. Accelerated 3D echo-planar spectroscopic imaging at 4 tesla using modified blipped phase-encoding. *Magn Reson Med*. 2007;58(5):1061-1066.
69. Lecocq A, Le Fur Y, Maudsley AA, et al. Whole-brain quantitative mapping of metabolites using short echo three-dimensional proton MRSI. *J Magn Reson Imaging*. 2015;42(2):280-289.
70. Althaus M, Dreher W, Geppert C, Leibfritz D. Fast 3D echo planar SSFP-based ^{1}H spectroscopic imaging: demonstration on the rat brain in vivo. *Magn Reson Imaging*. 2006;24(5):549-555.
71. Du W, Fan X, Foxley S, et al. Comparison of high-resolution echo-planar spectroscopic imaging with conventional MR imaging of prostate tumors in mice. *NMR Biomed*. 2005;18(5):285-292.
72. Hyder F, Renken R, Rothman DL. In vivo carbon-edited detection with proton echo-planar spectroscopic imaging (ICED PEPSI): [3,4-$^{13}CH_2$]glutamate/glutamine tomography in rat brain. *Magn Reson Med*. 1999;42(6):997-1003.
73. Du W, Karczmar GS, Uftring SJ, Du YP. Anatomical and functional brain imaging using high-resolution echo-planar spectroscopic imaging at 1.5 tesla. *NMR Biomed*. 2005;18(4):235-241.
74. Labadie C, Hetzer S, Schulz J, Mildner T, Aubert-Frecon M, Moller HE. Center-out echo-planar spectroscopic imaging with correction of gradient-echo phase and time shifts. *Magn Reson Med*. 2013;70(1):16-24.
75. Tsai SY, Posse S, Lin YR, et al. Fast mapping of the T_2 relaxation time of cerebral metabolites using proton echo-planar spectroscopic imaging (PEPSI). *Magn Reson Med*. 2007;57(5):859-865.
76. Ulrich M, Wokrina T, Ende G, Lang M, Bachert P. ^{31}P-{^{1}H} echo-planar spectroscopic imaging of the human brain in vivo. *Magn Reson Med*. 2007;57(4):784-790.

77. Wilhelm T, Bachert P. *In vivo* ^{31}P echo-planar spectroscopic imaging of human calf muscle. *J Magn Reson*. 2001;149(1):126-130.
78. Cunningham CH, Vigneron DB, Chen AP, et al. Design of flyback echo-planar readout gradients for magnetic resonance spectroscopic imaging. *Magn Reson Med*. 2005;54(5):1286-1289.
79. Chen AP, Cunningham CH, Ozturk-Isik E, et al. High-speed 3T MR spectroscopic imaging of prostate with flyback echo-planar encoding. *J Magn Reson Imaging*. 2007;25(6):1288-1292.
80. Srinivasan R, Cunningham C, Chen A, et al. TE-averaged two-dimensional proton spectroscopic imaging of glutamate at 3 T. *Neuroimage*. 2006;30(4):1171-1178.
81. Zhao C, Bolan PJ, Royce M, et al. Quantitative mapping of total choline in healthy human breast using proton echo planar spectroscopic imaging (PEPSI) at 3 tesla. *J Magn Reson Imaging*. 2012;36(5):1113-1123.
82. Greiser A, von Kienlin M. Efficient *k*-space sampling by density-weighted phase-encoding. *Magn Reson Med*. 2003;50(6):1266-1275.
83. Furuyama JK, Wilson NE, Thomas MA. Spectroscopic imaging using concentrically circular echo-planar trajectories in vivo. *Magn Reson Med*. 2012;67(6):1515-1522.
84. Schirda CV, Tanase C, Boada FE. Rosette spectroscopic imaging: optimal parameters for alias-free, High Sensitivity Spectroscopic Imaging. *J Magn Reson Imaging*. 2009;29(6):1375-1385.
85. Adalsteinsson E, Star-Lack J, Meyer CH, Spielman DM. Reduced spatial side lobes in chemical-shift imaging. *Magn Reson Med*. 1999;42(2):314-323.
86. Sarkar S, Heberlein K, Hu X. truncation artifact reduction in spectroscopic imaging using a dual-density spiral k-space trajectory. *Magn Reson Imaging*. 2002;20(10):743-757.
87. Kim DH, Adalsteinsson E, Spielman DM. Spiral readout gradients for the reduction of motion artifacts in chemical shift imaging. *Magn Reson Med*. 2004;51(3):458-463.
88. Andronesi OC, Gagoski BA, Sorensen AG. Neurologic 3D MR spectroscopic imaging with low-power adiabatic pulses and fast spiral acquisition. *Radiology*. 2012;262(2):647-661.
89. Hiba B, Faure B, Lamalle L, Decorps M, Ziegler A. Out-and-in spiral spectroscopic imaging in rat brain at 7 T. *Magn Reson Med*. 2003;50(6):1127-1133.
90. Levin YS, Mayer D, Yen YF, Hurd RE, Spielman DM. Optimization of fast spiral chemical shift imaging using least squares reconstruction: application for hyperpolarized ^{13}C metabolic imaging. *Magn Reson Med*. 2007;58(2):245-252.
91. Mayer D, Yen YF, Levin YS, et al. In vivo application of sub-second spiral chemical shift imaging (CSI) to hyperpolarized 13C metabolic imaging: comparison with phase-encoded CSI. *J Magn Reson*. 2010;204(2):340-345.
92. Josan S, Yen YF, Hurd R, Pfefferbaum A, Spielman D, Mayer D. Application of double spin echo spiral chemical shift imaging to rapid metabolic mapping of hyperpolarized [1-^{13}C]-pyruvate. *J Magn Reson*. 2011;209(2):332-336.
93. Josan S, Spielman D, Yen YF, Hurd R, Pfefferbaum A, Mayer D. Fast volumetric imaging of ethanol metabolism in rat liver with hyperpolarized [1-^{13}C] pyruvate. *NMR Biomed*. 2012;25(8):993-999.
94. Wiesinger F, Weidl E, Menzel MI, et al. IDEAL spiral CSI for dynamic metabolic MR imaging of hyperpolarized [1-^{13}C]pyruvate. *Magn Reson Med*. 2012;68(1):8-16.
95. Josan S, Hurd R, Park JM, et al. Dynamic metabolic imaging of hyperpolarized [2- C] pyruvate using spiral chemical shift imaging with alternating spectral band excitation. *Magn Reson Med*. 2014;71(6):2051-2058.
96. Seeger M, Nickisch H, Pohmann R, Scholkopf B. Optimization of *k*-space trajectories for compressed sensing by Bayesian experimental design. *Magn Reson Med*. 2010;63(1):116-126.
97. Uribe S, Mir R, Guesalaga A, Spiniak J, Irarrazaval P. A simple 3D k-space trajectory design method for MRSI and MRI applications. Poster presented at: 13th ISMRM Annual Meeting; 2005:2518, Miami, FL.
98. Uribe S, Guesalaga A, Mir R, Guarini M, Irarrazaval P. A 3D trajectory for undersampling *k*-space in MRSI applications. *Magn Reson Imaging*. 2007;25(3):350-358.
99. Ponder SL. Twieg DB. A novel sampling method for ^{31}P spectroscopic imaging with improved sensitivity, resolution, and sidelobe suppression. *J Magn Reson B*. 1994;104(1):85-88.
100. Banerjee S, Ozturk-Isik E, Nelson SJ, Majumdar S. Elliptical magnetic resonance spectroscopic imaging with GRAPPA for imaging brain tumors at 3 T. *Magn Reson Imaging*. 2009;27(10):1319-1325.
101. Scheenen TW, Klomp DW, Roll SA, Futterer JJ, Barentsz JO, Heerschap A. Fast acquisition-weighted three-dimensional proton MR spectroscopic imaging of the human prostate. *Magn Reson Med*. 2004;52(1):80-88.
102. Blaimer M, Breuer F, Mueller M, Heidemann RM, Griswold MA, Jakob PM. SMASH, SENSE, PILS, GRAPPA: how to choose the optimal method. *Top Magn Reson Imaging*. 2004;15(4):223-236.
103. Pruessmann KP, Weiger M, Scheidegger MB, Boesiger P. SENSE: Sensitivity encoding for fast MRI. *Magn Reson Med*. 1999;42(5):952-962.
104. Poole VN, Abbas K, Shenk TE, et al. MR spectroscopic evidence of brain injury in the non-diagnosed collision sport athlete. *Dev Neuropsychol*. 2014;39(6):459-473.
105. Dydak U, Meier D, Lamerichs R, Boesiger P. Trading spectral separation at 3T for acquisition speed in multi spin-echo spectroscopic imaging. *Am J Neuroradiol*. 2006;27(7):1441-1446.
106. Dydak U, Schar M. MR spectroscopy and spectroscopic imaging: comparing 3.0 T versus 1.5 T. *Neuroimaging Clin N Am*. 2006;16(2):269-283. x
107. Smith MA, Gillen J, McMahon MT, Barker PB, Golay X. Simultaneous water and lipid suppression for in vivo brain spectroscopy in humans. *Magn Reson Med*. 2005;54(3):691-696.
108. Balchandani P, Spielman D. Fat suppression for ^{1}H MRSI at 7T using spectrally selective adiabatic inversion recovery. *Magn Reson Med*. 2008;59(5):980-988.
109. Boer VO, van de Lindt T, Luijten PR, Klomp DW. Lipid suppression for brain MRI and MRSI by means of a dedicated crusher coil. *Magn Reson Med*. 2015;73(6):2062-2068.

110. Ebel A, Govindaraju V, Maudsley AA. Comparison of inversion recovery preparation schemes for lipid suppression in ^{1}H MRSI of human brain. *Magn Reson Med*. 2003;49(5):903-908.

111. Esmaeili M, Bathen TF, Rosen BR, Andronesi OC. Three-dimensional MR spectroscopic imaging using adiabatic spin echo and hypergeometric dual-band suppression for metabolic mapping over the entire brain. *Magn Reson Med*. 2017;77(2):490-497.

112. Hangel G, Strasser B, Povazan M, et al. Lipid suppression via double inversion recovery with symmetric frequency sweep for robust 2D-GRAPPA-accelerated MRSI of the brain at 7 T. *NMR Biomed*. 2015;28(11):1413-1425.

113. Ma C, Lam F, Johnson CL, Liang ZP. Removal of nuisance signals from limited and sparse ^{1}H MRSI data using a union-of-subspaces model. *Magn Reson Med*. 2016;75(2):488-497.

114. Osorio JA, Xu D, Cunningham CH, et al. Design of cosine modulated very selective suppression pulses for MR spectroscopic imaging at 3T. *Magn Reson Med*. 2009;61(3):533-540.

115. Ozhinsky E, Vigneron DB, Nelson SJ. Improved spatial coverage for brain 3D PRESS MRSI by automatic placement of outer-volume suppression saturation bands. *J Magn Reson Imaging*. 2011;33(4):792-802.

116. Sacolick LI, Rothman DL, de Graaf RA. Adiabatic refocusing pulses for volume selection in magnetic resonance spectroscopic imaging. *Magn Reson Med*. 2007;57(3):548-553.

117. Zhu H, Ouwerkerk R, Barker PB. Dual-band water and lipid suppression for MR spectroscopic imaging at 3 tesla. *Magn Reson Med*. 2010;63(6):1486-1492.

118. Bonekamp D, Smith MA, Zhu H, Barker PB. Quantitative SENSE-MRSI of the human brain. *Magn Reson Imaging*. 2010;28(3):305-313.

119. Dydak U, Possanzini C, Kozerke S, et al. 3D SENSE spectroscopic imaging with acceleration in three dimensions. *Proc. Intl. Soc. Mag. Reson. Med*. 2006;4:67.

120. Ozturk-Isik E, Crane JC, Cha S, Chang SM, Berger MS, Nelson SJ. Unaliasing lipid contamination for MR spectroscopic imaging of gliomas at 3T using sensitivity encoding (SENSE). *Magn Reson Med*. 2006;55(5):1164-1169.

121. Griswold MA, Jakob PM, Heidemann RM, et al. Generalized autocalibrating partially parallel acquisitions (GRAPPA). *Magn Reson Med*. 2002;47(6):1202-1210.

122. Raghavan RS, Panda A, Valette J, et al. 31P spectrocopic imaging with GRAPPA. *Proc. Intl. Soc. Mag. Reson. Med*. 2009;17:4317.

123. Young R, Serrai H. Implementation of three-dimensional wavelet encoding spectroscopic imaging: in vivo application and method comparison. *Magn Reson Med*. 2009;61(1):6-15.

124. Panych LP. Theoretical comparison of Fourier and wavelet encoding in magnetic resonance imaging. *IEEE Trans Med Imaging*. 1996;15(2):141-153.

125. Fu Y, Serrai H. Wavelet encoding spectroscopic imaging in small FOV regime: comparison to chemical shift imaging at 3 tesla. *Appl Magn Reson*. 2012;43(3):11.

126. Fu Y, Ijare O, Thomas G, Fazel-Rezai R, Serrai H. Implementation of wavelet encoding spectroscopic imaging technique on a 3 Tesla whole body MR scanner: in vitro results. In: *2009 Annual International Conference of the IEEE Engineering in Medicine and Biology Society (EMBC 2009)*. IEEE; 2009:2688-2691.

127. Fu Y, Serrai H. High speed magnetic resonance spectroscopic imaging using wavelet encoding and parallel imaging. *Proc Int Soc Magn Reson Med*. 2008;16:1582.

128. Lustig M, Donoho D, Pauly JM, Sparse MRI. The application of compressed sensing for rapid MR imaging. *Magn Reson Med*. 2007;58(6):1182-1195.

129. Cao P, Wu EX. accelerating phase-encoded proton MR spectroscopic imaging by compressed sensing. *J Magn Reson Imaging*. 2015;41(2):487-495.

130. Vidya Shankar R, Agarwal S, Geethanath S, Kodibagkar VD. Rapid MR spectroscopic imaging of lactate using compressed sensing. In: *Proceedings Volume 9417, Medical Imaging 2015: Biomedical Applications in Molecular, Structural, and Functional Imaging*; 2015:94171J https://doi.org/10.1117/12.2084003

131. Sarma MK, Nagarajan R, Macey PM, et al. Accelerated echo-planar J-resolved spectroscopic imaging in the human brain using compressed sensing: a pilot validation in obstructive sleep apnea. *Am J Neuroradiol*. 2014;35(Suppl 6):S81-S89.

132. Thomas MA, Nagarajan R, Huda A, et al. Multidimensional MR spectroscopic imaging of prostate cancer in vivo. *NMR Biomed*. 2014;27(1):53-66.

133. Nagarajan R, Iqbal Z, Burns B, et al. Accelerated echo planar *J*-resolved spectroscopic imaging in prostate cancer: a pilot validation of non-linear reconstruction using total variation and maximum entropy. *NMR Biomed*. 2015;28(11):1366-1373.

134. Goldstein T, Osher S. The split Bregman method for L1-regularized problems. *SIAM J Imaging Sci*. 2009;2(2):323-343.

135. Hu S, Lustig M, Chen AP, et al. Compressed sensing for resolution enhancement of hyperpolarized ^{13}C flyback 3D-MRSI. *J Magn Reson*. 2008;192(2):258-264.

136. Feinberg DA, Turner R, Jakab PD, von Kienlin M. Echo-planar imaging with asymmetric gradient modulation and inner-volume excitation. *Magn Reson Med*. 1990;13(1):162-169.

137. Larson PE, Hu S, Lustig M, et al. Fast dynamic 3D MR spectroscopic imaging with compressed sensing and multiband excitation pulses for hyperpolarized ^{13}C studies. *Magn Reson Med*. 2011;65(3):610-619.

138. Park I, Hu S, Bok R, et al. Evaluation of heterogeneous metabolic profile in an orthotopic human glioblastoma xenograft model using compressed sensing hyperpolarized 3D 13C magnetic resonance spectroscopic imaging. *Magn Reson Med*. 2013;70(1):33-39.

139. Askin NC, Atis B, Ozturk-Isik E. Accelerated phosphorus magnetic resonance spectroscopic imaging using compressed sensing. In: *2012 Annual International Conference of the IEEE Engineering in Medicine and Biology Society*. San Diego, CA, USA: IEEE; 2012:1106-1109.

140. Parasoglou P, Feng L, Xia D, Otazo R, Regatte RR. Rapid 3D-imaging of phosphocreatine recovery kinetics in the human lower leg muscles with compressed sensing. *Magn Reson Med*. 2012;68(6):1738-1746.

141. Kampf T, Fischer A, Basse-Lusebrink TC, et al. Application of compressed sensing to in vivo 3D ^{19}F CSI. *J Magn Reson*. 2010;207(2):262-273.

142. Maguire ML, Geethanath S, Lygate CA, Kodibagkar VD, Schneider JE. Compressed sensing to accelerate magnetic resonance spectroscopic imaging: evaluation and application to ^{23}Na-imaging of mouse hearts. *J Cardiovasc Magn Reson*. 2015;17:45.

143. Vidya Shankar R, Hu H, Bikkamane Jayadev N, Chang JC, Kodibagkar VD. Undersampling strategies for compressed sensing accelerated MR spectroscopic imaging. *Proc SPIE*. 2017. 10137:101372I

144. Heikal AA, Wachowicz K, Fallone BG. MTF behavior of compressed sensing MR spectroscopic imaging. *Med Phys*. 2013;40(5):052302.
145. Dong Z, Zhang Y, Peterson BS. Combination of compressed sensing and SENSE for 1H MRSI: an initial result. Poster presented at: ISMRM 19th Annual Meeting & Exhibition; May 9, 2011:3430; Montreal, Canada.
146. Dydak U, Pruessmann KP, Weiger M, Tsao J, Meier D, Boesiger P. Parallel spectroscopic imaging with spin-echo trains. *Magn Reson Med*. 2003;50(1):196-200.
147. Eslami R. Jacob M. a novel parallel sparse MRSI reconstruction scheme. *Proc Int Soc Magn Reson Med*. 2011;19:2853.
148. Fu Y, Serrai H. Fast magnetic resonance spectroscopic imaging (MRSI) using wavelet encoding and parallel imaging: in vitro results. *J Magn Reson*. 2011;211(1):45-51.
149. Gu M, Liu C, Spielman DM. Parallel spectroscopic imaging reconstruction with arbitrary trajectories using k-space sparse matrices. *Magn Reson Med*. 2009;61(2):267-272.
150. Lin FH, Tsai SY, Otazo R, et al. Sensitivity-encoded (SENSE) proton echo-planar spectroscopic imaging (PEPSI) in the human brain. *Magn Reson Med*. 2007;57(2):249-257.
151. Mayer D, Kim DH, Spielman DM, Bammer R. Fast parallel spiral chemical shift imaging at 3T using iterative SENSE reconstruction. *Magn Reson Med*. 2008;59(4):891-897.
152. Medved M, Ivancevic MK, Olopade OI, Newstead GM, Karczmar GS. Echo-planar spectroscopic imaging (EPSI) of the water resonance structure in human breast using sensitivity encoding (SENSE). *Magn Reson Med*. 2010;63(6):1557-1563.
153. Posse S, Otazo R, Tsai SY, Yoshimoto AE, Lin FH. Single-shot magnetic resonance spectroscopic imaging with partial parallel imaging. *Magn Reson Med*. 2009;61(3):541-547.
154. Tsai SY, Otazo R, Posse S, et al. Accelerated proton echo planar spectroscopic imaging (PEPSI) using GRAPPA with a 32-channel phased-array coil. *Magn Reson Med*. 2008;59(5):989-998.
155. Zhu X, Ebel A, Ji JX, Schuff N. Spectral phase-corrected GRAPPA reconstruction of three-dimensional echo-planar spectroscopic imaging (3D-EPSI). *Magn Reson Med*. 2007;57(5):815-820.
156. Lam F, Liang ZP. A subspace approach to high-resolution spectroscopic imaging. *Magn Reson Med*. 2014;71(4):1349-1357.
157. Lam F, Ma C, Clifford B, Johnson CL, Liang ZP. High-resolution ^{1}H-MRSI of the brain using SPICE: data acquisition and image reconstruction. *Magn Reson Med*. 2016;76(4):1059-1070.
158. Goelman G. Fast Hadamard spectroscopic imaging techniques. *J Magn Reson B*. 1994;104(3):212-218.
159. Gonen O, Hu J, Stoyanova R, Leigh JS, Goelman G, Brown TR. Hybrid three dimensional (1D-Hadamard, 2D-chemical shift imaging) phosphorus localized spectroscopy of phantom and human brain. *Magn Reson Med*. 1995;33(3):300-308.
160. Goelman G, Subramanian VH, Leigh JS. Transverse Hadamard spectroscopic imaging technique. *J Magn Reson*. 1990;89:18.
161. Goelman G, Walter G, Leigh JS. Hadamard spectroscopic imaging technique as applied to study human calf muscles. *Magn Reson Med*. 1992;25(2):349-354.
162. Tal A, Goelman G, Gonen O. In vivo free induction decay based 3D multivoxel longitudinal Hadamard spectroscopic imaging in the human brain at 3 T. *Magn Reson Med*. 2013;69(4):903-911.
163. Gonen O, Arias-Mendoza F, Goelman G. 3D localized in vivo 1H Spectroscopy of human brain by using a hybrid of 1D-Hadamard with 2D-chemical shift imaging. *Magn Reson Med*. 1997;37(5):644-650.
164. Gonen O, Murdoch JB, Stoyanova R, Goelman G. 3D multivoxel proton spectroscopy of human brain using a hybrid of 8th-order Hadamard encoding with 2D chemical shift imaging. *Magn Reson Med*. 1998;39(1):34-40.
165. Cohen O, Tal A, Goelman G, Gonen O. Non-spin-echo 3D transverse Hadamard encoded proton spectroscopic imaging in the human brain. *Magn Reson Med*. 2013;70(1):7-15.
166. Cohen O, Tal A, Gonen O. Three-dimensional Hadamard-encoded proton spectroscopic imaging in the human brain using time-cascaded pulses at 3 tesla. *Magn Reson Med*. 2014;72(4):923-933.
167. Goelman G, Liu S, Hess D, Gonen O. Optimizing the efficiency of high-field multivoxel spectroscopic imaging by multiplexing in space and time. *Magn Reson Med*. 2006;56(1):34-40.
168. Ohliger MA, Larson PE, Bok RA, et al. Combined parallel and partial Fourier MR reconstruction for accelerated 8-channel hyperpolarized carbon-13 in vivo magnetic resonance spectroscopic imaging (MRSI). *J Magn Reson Imaging*. 2013;38(3):701-713.
169. Speck O, Scheffler K, Hennig J. Fast 31P chemical shift imaging using SSFP methods. *Magn Reson Med*. 2002;48(4):633-639.
170. Schuster C, Dreher W, Geppert C, Leibfritz D. Fast 3D ^{1}H spectroscopic imaging at 3 tesla using spectroscopic missing-pulse SSFP with 3D spatial preselection. *Magn Reson Med*. 2007;57(1):82-89.
171. Schuster C, Dreher W, Stadler J, Bernarding J, Leibfritz D. Fast three-dimensional 1H MR spectroscopic imaging at 7 tesla using "spectroscopic missing pulse-SSFP". *Magn Reson Med*. 2008;60(5):1243-1249.
172. Guo J, Patay Z, Reddick WE. Fast frequency-sweep spectroscopic imaging with an ultra-low flip angle. *Sci Rep*. 2016;6:30066.
173. Maudsley AA, Darkazanli A, Alger JR, et al. Comprehensive processing, display and analysis for in vivo MR spectroscopic imaging. *NMR Biomed*. 2006;19(4):492-503.
174. Wilson NE, Iqbal Z, Burns BL, Keller M, Thomas MA. Accelerated five-dimensional echo planar J-resolved spectroscopic imaging: implementation and pilot validation in human brain. *Magn Reson Med*. 2016;75(1):42-51.
175. Otazo R, Tsai SY, Lin FH, Posse S. Accelerated short-TE 3D proton echo-planar spectroscopic imaging using 2D-SENSE with a 32-channel array coil. *Magn Reson Med*. 2007;58(6):1107-1116.

How to cite this article: Vidya Shankar R, Chang JC, Hu HH, Kodibagkar VD. Fast data acquisition techniques in magnetic resonance spectroscopic imaging. *NMR in Biomedicine*. 2019;32:e4046. https://doi.org/10.1002/nbm.4046